ALEPH 91-27
PHYSIC 91-26
25.2.1991
J.C. Brient et al.

Forward-backward asymmetry in Z decays to $\tau^+\tau^-$

J.-C.Brient, S.Loucatos, P.S.Marrocchesi

February 22, 1991

Abstract

A^{τ}_{FB} is measured by three different analyses. The first one applies τ-pair selection used in the $\tau^+\tau^-$ cross-section determination and subtracts identified e^+e^- pairs. The other two use the ECAL and the HCAL to identify τ's and reduce e^+e^- contamination. The results of the three methods are in good agreement.

1 Introduction

The lepton forward-backward asymmetry depends on the neutral current Vector and Axial couplings. In Aleph, since the τ lepton is detected with a very good efficiency, the measurement of A^{τ}_{FB} allows a good determination of $g^2_{\mathrm{V}\ell}(M^2_{\mathrm{Z}})\ /g^2_{\mathrm{A}\ell}(M^2_{\mathrm{Z}})$.

The measurement of lepton A_{FB} on data of 89 and 90 up to mid May ($2.6pb^{-1}$) were published in [1] (Electroweak Paper). The $\tau^+\tau^-$ sample used for the measurement of A_{FB} has changed since the Electroweak paper, and due to improved statistics, a careful study of the systematics is now needed. Analysis of data up to mid of June 90 ($3.8pb^{-1}$) were shown at the Singapore conference. Here we present the results for the total 89+90 data. Three different analyses have been performed, following different approaches for the rejection of large angle e^+e^- background. The results show a good agreement among the three methods. The three analyses will be presented below, after a short discussion on the influence of background contamination on A_{FB} .

2 Expected influence of background on A^{τ}_{FB}

The size of the systematic error induced by different sources of background on A_{FB} has been estimated as follows .
For each pair of cos θ^* bins centered at x_i = cos θ^*_i and -x_i respectively, a differential asymmetry A_i can be defined as :

$$A_i = \frac{N_i^+ - N_i^-}{N_i^+ + N_i^-}$$

For $\tau^+\tau^-$ events we expect :

$$A_i = \frac{8}{3}\ A_{\rm FB}\ w_i$$

where :

$$w_i = \frac{x_i}{1+x_i^2}$$

Let B_i^+ and B_i^- be the number of background events in bins x_i and -x_i , respectively and $C_i = \frac{B_i^+ + B_i^-}{N}$ where $C^{bkg} = \sum_{i=1}^{n_b} C_i$ is the total background contamination from e^+e^- pairs ; n_b is the number of bin pairs ; N is the total number of selected $\tau^+\tau^-$ events.
The systematic error on $A_{\rm FB}$ due to the background is :

$$\delta A_{\rm FB} = -\sum_{i=1}^{n_b} C_i A_i + \sum_{i=1}^{n_b} C_i A_i^{bkg} = \sum_{i=1}^{n_b} C_i (A_i^{bkg} - A_i)$$

where :

$$A_i^{bkg} = \frac{B_i^+ - B_i^-}{B_i^+ + B_i^-}$$

and :

$$A^{bkg} = \sum_{i=1}^{n_b} A_i^{bkg} \frac{(N_i^+ + N_i^-)}{N}$$

is the asymmetry in the angular distribution of the background events .

The first term in $\delta A_{\rm FB}$ is due to background events with a forward-backward symmetrical distribution (e.g.: $\gamma\gamma$ events).
It contributes a total systematic error of :

$$\delta A_{\rm FB}/A_{\rm FB} = -C^{bkg}$$

which has the effect to compress by a multiplicative $(1-C)$ scale factor the $\sqrt{s}$ dependence of $A_{\rm FB}$.
The second term, due to asymmetrical backgrounds (e.g.: e^+e^- events) produces a ***signed*** (i.e. positive in the case of the t-channel contribution) shift in the measured value of $A_{\rm FB}$ of size :

$$\delta A_{\rm FB} = C^{bkg} A^{bkg}$$

3 Energy scan

In 1989 nine energy points were measured:

88.28, 89.29, 90.28, 91.03, 91.28, 91.53, 92.28, 93.29, 94.28 GeV

In 1990 seven points:

88.22, 89.22, 90.22, 91.22, 92.22, 93.22, 94.22 GeV

The error on the absolute LEP center-of-mass energy is ± 20 MeV and ± 10 MeV point to point. Only the latter is relevant in extracting the EW parameters from the asymmetries because the dominant term where it appears is a function of $(\sqrt{s} - M_z)$ near the pole (section 2).

The slope of A_{FB} as a function of $\sqrt{s}$ is $\leq$ 8% / GeV for the measured value of $g_{A\ell}(M_Z^2)$. Thus, scan points differring by $\sim$ 60 MeV can be averaged, weighted by integrated luminosities, and the effect on A_{FB} fits is negligible.

4 The simulations

The $\tau^+\tau^-$ production is simulated by KORL03 which contains up to 2nd order matrix elements. QED corrections in the decays of the tau which may have some uncertainties in the calculation, but this should not affect this analysis.

The process $e^+e^- \rightarrow e^+e^-$, which is the main source of systematics, is simulated by BHAB01, which is 1st order only. Double emission of real photons is not simulated.

5 Event preselection

In the selections it is required that all the parts of the detector that are used for this analysis are functioning and that all relevant triggers are enabled: the data sample used for the analysis of the A_{FB} of the $\tau^+\tau^-$ events , corresponds to any "PERF" and "MAYB" runs. The EW group decided, though, not to use some of these runs in the cross section analyses, mainly because they had low HCAL efficiency (first 89 runs).

Events are preselected using Class 15.

Each event is divided into two hemispheres by a plane perpendicular to the thrust axis. In each hemisphere we define a "jet" by clustering together all the charged tracks present in the hemisphere. The direction of the τ is defined by the vectorial sum of the momenta of all the tracks of the jet (the jet axis).

In the $\tau^+\tau^-$ decay the asymmetry measurement depends on the contamination from the e^+e^- pairs because of the strong forward asymmetry of the t-channel. Three different event selections have been used in order to suppress the remaining e^+e^- contamination. The first one takes advantage of the event selection used for the measurement of the $\tau^+\tau^-$ cross-section ([2]) with an additional rejection of identified e^+e^- pairs. The other two follow a complementary approach: the ECAL and the HCAL are used to lower the systematic uncertainties from e^+e^- contamination.

6 Selection using the missing mass and electron identification

6.1 Event selection

$\tau^+\tau^-$ events are first selected according to the criteria used for the measurement of the cross section (Ref. [2]).
For the asymmetry measurement a correct assignment of the charge of the lepton is required . The total reconstructed charge in the event from data is compared with the MC prediction in Fig. 1 . The distribution is symmetric for either charge sign and in good agreement with the prediction .
Events with non zero total charge have been studied both from data and MC .

The extra track which is present in events with 1+2 topology (mainly the result of interactions in the apparatus) is characterized by low momentum and large impact parameter. A cut on total zero charge is applied with a reduction of 8.5 $\pm$ 0.4 % in the number of events.

As explained in Ref. [2], the sample of events selected for the cross section measurement at the Z_0 peak is affected by a background contamination from e^+e^- of size 1.1$\pm$0.5 %.
We have further reduced the amount of such background by rejecting those events which are identified as e^+e^- pairs using the selection program of (Ref. [3]).
This selection takes advantage of the energy recovered in HCAL as a correction for the energy losses in ECAL due to the cracks . For events with one and only one charged track per hemisphere, the energies of the ECAL clusters (from a charged lepton or radiative photon) close to an ECAL crack are summed to the energy of those HCAL clusters which are found near the crack.
The main cut requires the corrected total energy to exceed the value of 1.11 $\sqrt{s}$.
The application of Bhabha rejection cuts , reduces the event sample to 99.3 % of the original one.

The efficiency of the e^+e^- rejection on the events accepted by the cross section selection has been evaluated by Monte Carlo simulation for different angular regions (Ref. [2]). The rather poor 50 % average efficiency for this particular class of e^+e^- events ($m_x^2 > 400\,GeV^2$, $E_{wires} < 55$ GeV) has to be compared with the average 98.4 % efficiency obtained on an unbiased e^+e^- sample .

If we assume an average e^+e^- rejection efficiency of 50 % for the events passing the τ selection cuts, we expect the systematic error induced by the residual e^+e^- background on A_{FB} at the peak to be of order -0.0017 .
The uncertainty on this correction is dominated by the uncertainty on the background contamination ΔC and by the uncertainty on the asymmetry of the background ΔA^{bkg}.

The value of A^{bkg} is measured from the data by binning the angular distribution of the e^+e^- identified events in 18 bins of $cos\theta^*$. By lowering the missing mass cut, the amount of background can be enhanced to get a statistically more accurate measurement

of A^{bkg}. At the peak, we find for the identified Bhabha events :

$$A^{bkg} = 0.30 \pm 0.06$$

with ($m_x^2 > 0\, GeV^2$, $E_{wires} < 55$ GeV) while we get :

$$A^{bkg} = 0.18 \pm 0.08$$

with ($m_x^2 > 400\, GeV^2$, $E_{wires} < 55$ GeV).

The value of C^{bkg} is inferred from the data by counting the number of events flagged as e^+e^- and by assuming a background rejection efficiency of 50% . The error ΔC^{bkg} on the total background contamination C^{bkg} (see table 2) is dominated by the statistical error and by the uncertainty on the Bhabha identification efficiency.

As a consistency check, the variation of the $\tau^+\tau^-$ asymmetry as a function of the amount of e^+e^- contamination can be observed directly from the data . By varying the missing mass cut on the data at the peak, we can add to our sample a known fraction of e^+e^- background and measure its effect on the value of the asymmetry . In Fig. 2 the observed variation of $\delta A_{\rm FB}$ of the asymmetry is shown as a function of the estimated background contamination . The low value of the e^+e^- efficiency for events with missing mass $> 400\ GeV^2$ is of little consequence here, as the largest variation of the asymmetry occurs for small values of the missing mass cut ($m_x^2 < 100\ GeV^2$) , where the e^+e^- identification efficiency is fairly high .

For each value of the missing mass cut, the value of the asymmetry is obtained by an unbinned maximum likelihood fit to the angular distribution .
However, if we do plot the data in 18 bins of $\cos\theta^*$ in the range [-0.9,+0.9] , we observe that *only* the upper bin at +0.9 gets more populated when the amount of e^+e^- background is increased by lowering the missing mass cut.

Table 1: Contamination from $\gamma\gamma$ events . Estimated correction to the measured asymmetry .

$\sqrt{s}$ (GeV)	$C_{\gamma\gamma}$ %	$\delta A_{\rm FB}^{\gamma\gamma}$ %
88.28	3.1 ± 1.3	-1.1 ± 0.5
89.28	3.2 ± 0.6	-0.3 ± 0.05
90.28	1.4 ± 0.3	-0.1 ± 0.02
91.28	0.8 ± 0.2	0.01 ± 0.002
92.28	1.2 ± 0.2	0.2 ± 0.03
93.28	2.3 ± 0.4	0.5 ± 0.1
94.28	3.1 ± 0.6	0.7 ± 0.3

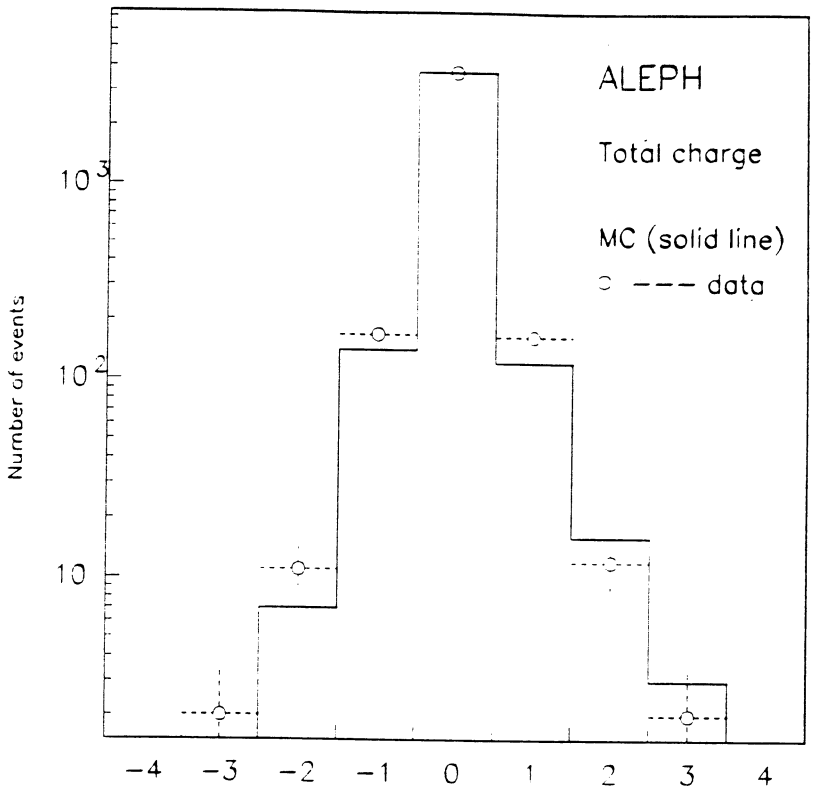

Figure 1: Number of events as a function of the total charge measured by the TPC for events passing the tau selection

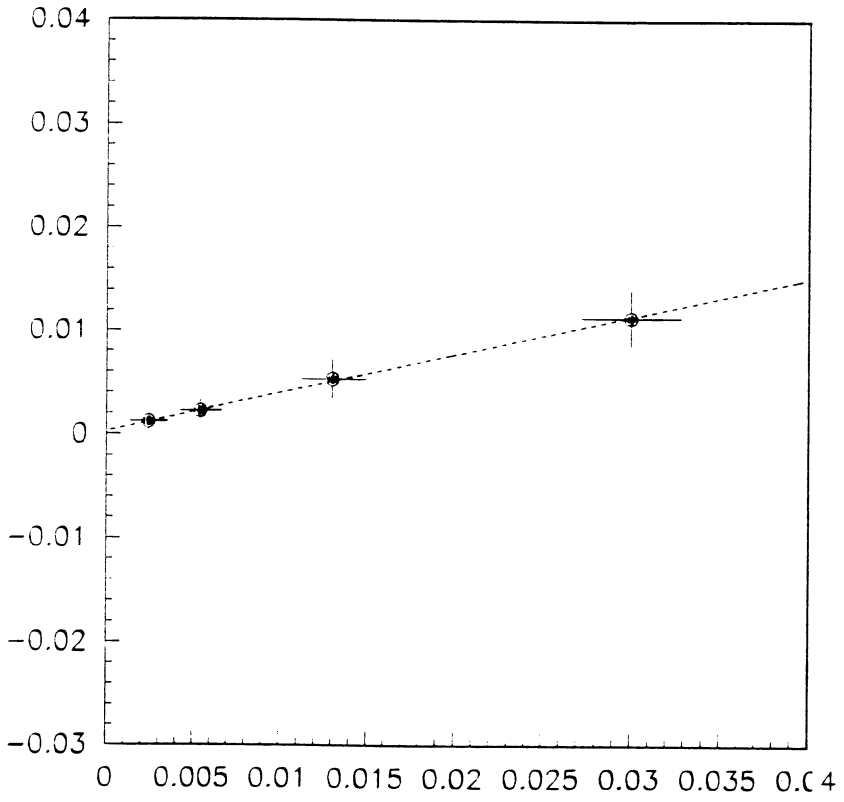

Figure 2: Variation of the measured value of the forward backward asymmetry as a function of the total percentage of e^+e^- background in the data

The slope from Fig. 2 is consistent with a background asymmetry A^{bkg} of 0.37 ± 0.1.

The contamination from $\gamma\gamma$ background at the peak was found to be 0.65 ± 0.12 % . By assuming a FB symmetrical $(1 + cos^2\theta)/sin^2\theta$ angular distribution for this background, the required correction to A_{FB} due to a total percentual contamination C^{bkg} of $\gamma\gamma$ events is :

$$\delta A_{FB}/A_{FB} = -C^{bkg}$$

This would result in a negligible correction of $\delta A \simeq -10^{-4}$ to the measured A_{FB} value at the peak . Outside the resonance, we expect the background to signal ratio to increase to about 3.1 % at $\sqrt{s} = 88.28\ GeV$.
The required correction on the asymmetry at this point would be δA = -1.1 % which has to be compared with the predicted value for the asymmetry of -27.4% and the current statistical error of 9.4 %

The values for the correction applied at each CM energy point for the combined fit to 1989 and 1990 data are listed in table 2 together with the estimated uncertainty on the correction .

6.2 Fit procedure

The number of events selected per cms energy point are listed in table 2 for the combined '89 and '90 data, together with their statistical errors. An unbinned maximum likelihood fit to the angular distribution is performed for each energy . The measured values of A_{FB}, before and after the correction for the residual e^+e^- background, are listed in table 2.

The fit has been repeated , introducing an additional free parameter $\mathbf{a_2}$ for the curvature term $cos^2\theta^*$:

$$N(1 + \mathbf{a_2}\ cos^2\theta^* + \frac{8}{3}\ A_{FB}\ cos\theta^*)$$

The effect on A_{FB} at the peak is negligible : 0.0132 ± 0.016 with $\mathbf{a_2}$ as a free parameter to be compared with 0.0133 ± 0.016 with the same parameter constrained to 1.

Figure 3. Measured values of the forward backward asymmetry A_{FB} as a function of CM energy . The dotted line is the result of a fit to $a_e * a_\tau$, $v_e * v_\tau$ coupling constants .

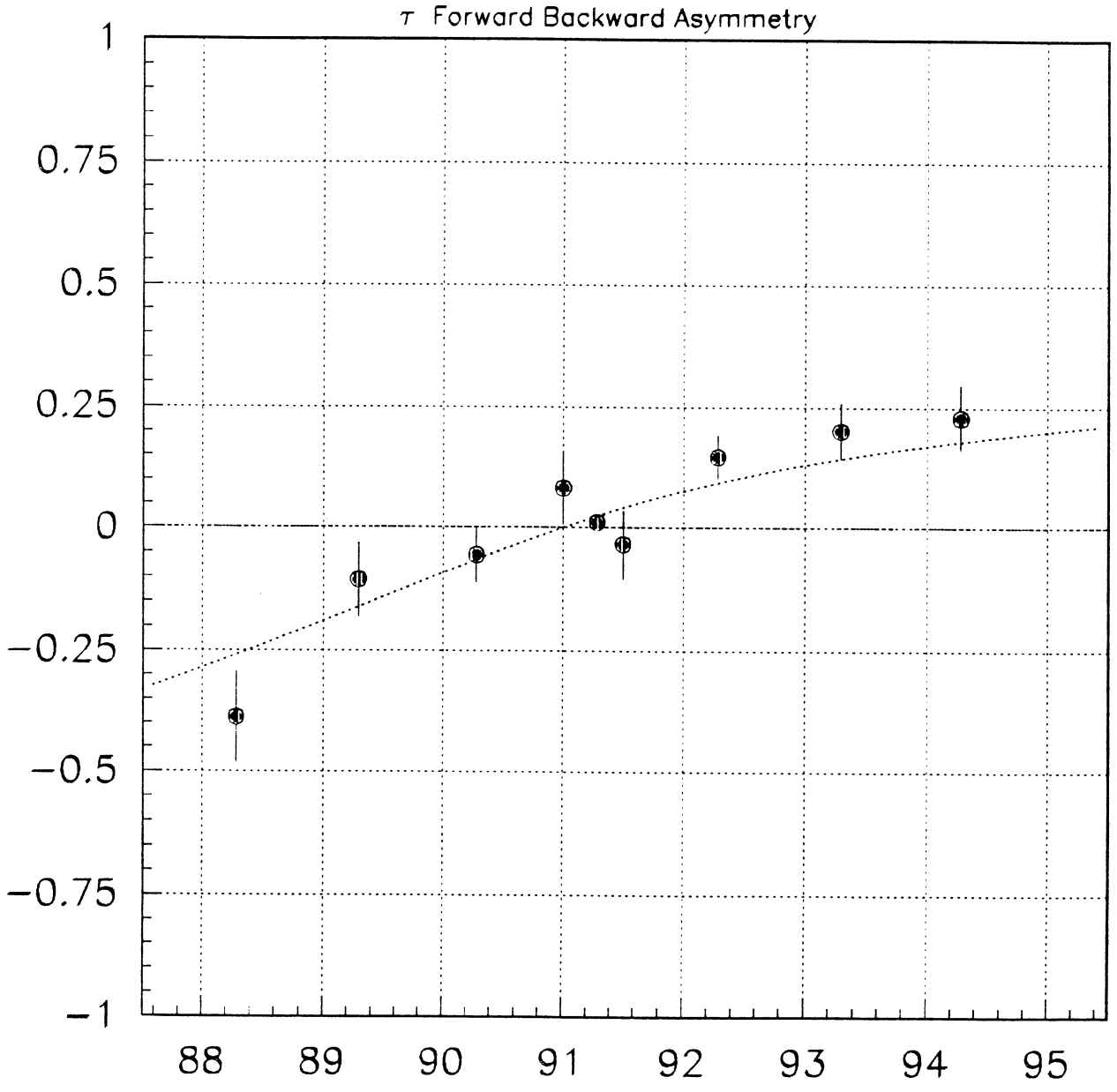

Table 2: Measured values of A_{FB} vs. cms energy before and after background correction
*

$\sqrt{s}$ (GeV)	events	C^{Bhabha} (%)	$\delta A_{Bhab.}$ (%)	A_{FB}^{meas} (%)	A_{FB}^{corr} (%)
88.28	84	1.2±1.2	−1.1±0.7	−36.6±9.4	−38.8 ±9.4 ±0.9
89.28	170	0.6±0.6	−0.4±0.4	−9.9±7.5	−10.6 ±7.5 ±0.4
90.28	344	0.9±0.5	−0.5±0.3	−5.0±5.5	−5.6 ±5.5 ±0.3
91.03	168	0.3±0.4	−0.06±0.1	+8.3±7.5	+8.2 ±7.5 ±0.1
91.28	3902	0.6±0.1	−0.17±0.03	+1.3±1.6	+1.1 ±1.6 ±0.03
91.53	185	0.5±0.5	−0.10±0.1	−3.3±7.0	−3.4 ±7.0 ±0.1
92.28	481	0.8±0.4	−0.31±0.2	+14.8±4.4	+14.7 ±4.4 ±0.2
93.28	264	0.2±0.3	−0.11±0.2	+20.6±5.7	+20.1 ±5.7 ±0.2
94.28	204	0.1±0.1	−0.04±0.4	+22.2±6.6	+22.8 ±6.6 ±0.4

*

7 Selection using the Ecal

This selection is also described in [4].

7.1 Pre-selection

The runs with good condition of the detector ("perf" and "mayb") used for the cross section by the Electroweak group have also been used, except, because of the importance of the ECAL detector in this analysis, runs with problems in ECAL. However, when only some modules have problems , only events with tracks crossing one of the bad modules are not used. In order to have no ambiguity on the charge of the τ , events are "pre-selected" if the two hemispheres have opposite charge signs. The angular acceptance for the polar angle is restricted to $|\cos\theta^*| < 0.9$. (θ^* is defined in section 8.5). To separate the $\tau^+\tau^-$ from the $Z \rightarrow \mu\mu\gamma's$ and 2-photon process, specific rejections have been done. The 2-photon rejection is based on acolinearity and on the sum of the transverse momentum (TPC). The $\mu\mu$ rejection is based on the missing mass squared and the muon identification in HCAL and muon-chambers. (these rejections are the standard ones of the updated version of the program TAUSEL). After this filtering, the data sample contains the $\tau^+\tau^-$ and the Bhabha events, with a small background of $Z \rightarrow \mu\mu\gamma's$ and 2-photon process. What is called Bhabha event here is not only the QED process (t-channel) but all the "quasi" two-body reactions with $e^+e^-\gamma$'s final state. (i.e. $Z \rightarrow e^+e^-\gamma's$).

The analysis presented here rejects the Bhabha events with a positive identification of the $\tau^+\tau^-$, based on the muon and pion identification. The selection is done in such a way that the amount of Bhabha background can be measured directly from the data. The positive identification of the $\tau^+\tau^-$ leaves the Bhabha background unchanged in case of malfunction of one part of the detector (i.e HCAL problem would create an extra rejection of $\tau^+\tau^-$ but not an increase on the number of Bhabha background).

7.2 track identification

7.2.1 μ definition

The definition is based on the penetration of the track, in the outer part of HCAL. A road of 2.5 cm $\pm 3\sigma$(multiple scattering) is defined around the extrapolation of the charged track. In the road, the tracks must fire at least 2 planes in the last 10 planes of HCAL.

7.2.2 $\pi^{\pm}$ definition

A pion is defined as a minimum ionizing particle which is not a muon. The definition of the minimum ionizing particle in the ECAL, is based on the energy deposition in the tower crossed by the charged track. Any track compatible (at 3 σ), with a minimum ionizing particle in the first stack, is declared "pion" (program ECALMU). Due to the problem to define the first stack in the ECAL overlap region, the cut is extended to stacks 1 and 2. To avoid some problem of extrapolation of the track in the first stack of ECAL, a minimum momentum of 3 GeV/c is required. For the tracks with momentum from 0.5 to 3. GeV/c, the dE/dx of the TPC is used. Figure 15 shows the scatter plot of the number of σ for the electron hypothesis versus the number of σ for the π hypothesis. The straigth line defines the region of identified pions (pion region is below the line). For the intermediate region (3 to 6 GeV/c), any track called "pion" by the ECAL definition, must also be in the allowed region for pions in the dE/dx of the TPC (below the dotted line in figure 15).

7.2.3 π^o definition

The photon identification algorithm by A.Rougé has been used, with a minimum energy for each photon of 250 MeV/c, and 4 cm as the minimum distance between the photon and the nearest impact of a charged track in stack 1. When less than 5 γ are found in one hemisphere, all combinations of 2 γ with momentum $P_{\gamma\gamma} < 20$ GeV/c are considered. π^o are identified when the $\gamma\gamma$ mass is between 90 and 200 MeV. Just to have a picture of the π^o reconstruction quality, a τ is selected in one hemisphere (Low ECAL energy and at least one charged pion identified), and the mass $\gamma\gamma$ closest to the mass of the π^o is plotted in the other hemisphere (histogram in figure 16). Doing the same with Bhabha events (large ECAL energy and not low TPC energy in one hemisphere), we obtain the shaded histogram in figure 16. The ratio signal/noise is reasonably large in the region 90 to 200 MeV.

7.3 $\tau^+\tau^-$ selection

The logic of the selection is the following :
• for each good track
— if Ptpc > 3. GeV/c try μ identification
— if the track is not identified as μ, try π identification

The number of pions is defined as the sum of the neutral and charged ones. Tagging Bhabha events in one hemisphere, allows to use the other one to have an unbiased "one hemisphere sample" of Bhabhas. Using this "one hemisphere sample" of Bhabhas, we

can have the probability Prob(nπ) to identify n π per hemisphere for the Bhabha events. Figures 18 to 20 show these probability distributions in the different geometrical regions of ECAL.

From these distributions, one can conclude that the most important background arises when only one π is identified in the event. Finally, the selected $\tau^+\tau^-$ samples contains the two samples **class I** and **class II**, defined by:

	Selections
Class I	≥ 1 μ Id. **OR** ≥ 2 π Id.
Class II	Only 1 π Id. but for each Hemisph. E^{wires}_{ECAL} / E_{beam}<0.8

In order to show the average efficiency of π/μ idenfication to separate Bhabha, $\tau^+\tau^-$ and $\mu^+\mu^-$, the sample is integrated over the polar angle cosθ^*. The distributions of figure 17 show the probability Prob(nπ) for the three different tag sample. The global efficiency including geometrical acceptance, to select $\tau^+\tau^-$ events, is 68.2 %

7.4 Bhabha background

7.4.1 method of estimation

The estimation of the Bhabha background in the $\tau^+\tau^-$ sample, is obtained from the "one hemisphere sample" of Bhabhas. This sample depends on the tag definition of this type of events. This tag definition is a compromise between the efficiency to tag Bhabha event and the contamination of $\tau^+\tau^-$ event in the " tag Bhabha " sample.

Bhabha Tag definition : • $P_{TPC} > 0.3E_{beam}$ .and. $E_{ECAL} > 0.8E_{beam}$

For each ECAL region, the efficiency to tag the Bhabhas is computed from the single and double tag Bhabha sample. Applying this efficiency to the tagged Bhabhas leads to the total number of Bhabhas for each ECAL region.

For **class I**, the remaining Bhabha background is then computed from the total number of Bhabha and from the probability to have, in Bhabha events, at least 2 pions identified per event (figures 18 to 20).

For **class II**, we need to have the value of the ECAL energy cut efficiency for Bhabha. The E^{wires}_{ECAL} / E_{beam}distribution is plotted for one hemisphere, when the other is a tagged Bhabha, and when the event contains exactly one pion. Figures 21 to 23 show these distributions for the different regions of ECAL. The efficiency of the energy cut is then derived from these distributions. In the hypothesis of non-correlation from one hemisphere to the other one (see paragraph 5.2.3 and 5.2.4), the number of Bhabhas remaining in the $\tau^+\tau^-$ sample is given by :

$$N_{Bhabha}(\textbf{classI}) = 2. * Prob(\geq 2\pi) * Nreg. \quad (1)$$

$$N_{Bhabha}(\textbf{classII}) = 2. * Prob(1\pi) * Prob(ECALcut) * Nreg. \quad (2)$$

where $Prob(n\pi)$ is the probability to have n π identified per hemisphere in a Bhabha event (figures 18 to 20), Prob(ECAL cut) is the probability to have **one** of the hemispheres which fails the ECAL cut (related to figure 21 to 23), and Nreg is the number of Bhabhas for each geometrical region of ECAL (Barrel,etc...) The factor 2 corresponds to the possiblity to have 1 π in each hemisphere. Table I summarizes the number of Bhabha background events estimated for each ECAL region

	Barrel	Overlap	End-Cap
Class I	$5.8\ ^{+5.7}_{-4.7}$	$1.6\ ^{+2.7}_{-1.6}$	$2.3\ ^{+2.4}_{-2.3}$
Class II	3.2 ± 2.5	0.6 ± 0.4	0.6 ± 0.6

Table I
Estimated Bhabha background

The total number of Bhabha background events in the $\tau^+\tau^-$ sample , is $14.1\ ^{+7.2}_{-5.9}$

7.4.2 Systematics on Bhabha background

Check in the plane ECAL energy vs TPC energy

The charged tracks energy of the events has not been used in the selection, and we can now plot it versus the ECAL total energy to see if there is an accumulation in the region where the background is expected (figure 24). No clear accumulation is observed, except in the region corresponding to $\mu^+\mu^-$ (low ECAL energy and large TPC energy). Now, $\tau^+\tau^-$ Monte Carlo, and the real data can be compared in two interesting regions

- large ECAL energy (E > 40 GeV)
- large TPC energy (E > $0.5\sqrt{s}$)

In the large ECAL energy region two distributions have been used. First, the TPC energy normalized to $\sqrt{s}$. Figure 26 shows this distribution for real data (points with error bars) and for $\tau^+\tau^-$ M.C. (histogramm). An excess of the order of 16. $\pm$4.5 events is observed in the region E(TPC)>$0.8\sqrt{s}$. A second distribution used is the missing mass squared distribution, shown in figure 27. After $\tau^+\tau^-$ M.C. normalization, an excess of 18. $\pm$11. events is observed in the region $|MM^2|$ <$400.GeV^2$.

In the large TPC energy region, the total ECAL energy distribution has been used. Figure 28 shows this distribution for real data (points with error bars) and the prediction of the $\tau^+\tau^-$ M.C. (histogramm). In the region Eecal >$0.75\sqrt{s}$, an excess of 9. $\pm$4. events is observed. In this figure the $\mu^+\mu^-$ remaining background can also be seen as an excess of events at low ECAL energy.

In conclusion, the study of the population in the plane ECAL energy versus TPC energy, gives a set of numbers for the Bhabha background reasonably consistent with the calculated number of 14.1.

The ECAL energy vs TPC energy plane gives also information on the other backgrounds. As mentionned above, an accumulation is visible in the $\mu^+\mu^-$ region. Figure 25 shows the TPC energy for events with low ECAL energy (below 5 GeV). A clear peak is observed above $0.9\sqrt{s}$, but also a slight excess below $0.2\sqrt{s}$, corresponding to the remaining $\gamma\gamma$ background. In order to reject the remaining background of mu pairs, when the total ECAL energy is smaller than $0.1\ \sqrt{s}$, events with total TPC energy larger than $0.9\sqrt{s}$ are rejected. For the 2-photon background, an excess of 68 $\pm$18 events is observed at low TPC energy. This number is in agreement with the background of 53 $\pm$13 events, calculated from the density in the plane acolinearity vs $\sum P_{tpc}$, before the rejection of $\gamma\gamma$ events.

Systematics related to the Bhabha tag definition

A priori, the e/π misidentification in the Bhabha tag sample does not depend on the tag definition. However, if there is any correlation between the tag definition and Prob(nπ), as small as it can be, that could generate a bias in the number of e/π misidentification per hemisphere. In order to check it, the cut on ECAL energy in the tag definition has been changed from 0.7 Ebeam to 0.95 Ebeam. Below 0.8 Ebeam, an additional cut on the missing mass squared at 800 GeV^2 is performed (which is not related to the ECAL identification of pions), to keep constant the level of the $\tau^+\tau^-$ background in the tag Bhabha sample. Figure 29 shows the variation of the e/π misidentification, as a function of the cut on E_{ECAL}, for the three regions of ECAL (Barrel,Overlap and End-Cap). No significant variation is observed. The mean value for each region has been used for the Prob(π number).The error on this probability has been calculated as the maximum variation (including the statistical error bars, which is a conservative choice) in the range of the tag definition. Table II shows the values used for the probabilities for each ECAL region, and the errors on these numbers.

	Barrel	Overlap	End-Cap
Prob (1π) (10^{-3})	$5.5\ ^{+2.2}_{-1.3}$	$6.2\ ^{+4.2}_{-3.2}$	$7.0\ ^{+1.8}_{-2.0}$
Prob ($\geq$ 2π) (10^{-4})	$5.3\ ^{+5.3}_{-4.3}$	$6.0\ ^{+10.0}_{-6.0}$	$3.9\ ^{+4.1}_{-3.9}$

Table II
Number of misidentification e/π per hemisphere for Bhabha

Systematics related to e/π misidentification

In formulae (1) and (2), the probability of e/π misidentification is assumed to have no correlation from one hemisphere to the other. To check this hypothesis, the ECAL energy cut is removed in CLASS II. The number of Bhabhas in the new sample is then calculated only from the probability of misidentification, with the hypothesis of non-correlation, and formulae (1) and (2) give a number of 122 $\pm$29 events. The same number is measured by making the difference between the new sample (corrected for non Bhabha background

and the increased selection efficiency for $\tau^+\tau^-$ events) and the old sample (with ECAL energy cut in class II).

The number is 104 $\pm$12 events, in reasonable agreement with the calculated one. We estimate that the non-correlation hypothesis introduces a systematic of $\pm$15 %, on the number of Bhabhas calculated from formulae (1) and (2).

Systematics related to ECAL energy

To estimate the systematics on the Bhabha rejection due to the ECAL energy cut in class II, the value of the cut has been changed from $0.8E_{beam}$ to $0.95E_{beam}$ (for this value, there is a significant variation on the number of Bhabha).The calculated number of Bhabha, with formula (1) and (2), is 43 $\pm$10 events. Following the same procedure as in the previous paragraph, we obtain from the data 24 $\pm$12, leading to $\pm$44 % as the systematics on the values of Bhabha background quoted in class II.

7.4.3 Conclusion about Bhabha background

Including the systematics, the Bhabha background is :

$$\textbf{class I } N_{Bhabha} = 9.7\ ^{+6.7}_{-5.5}\ (\text{S1})\ \pm 1.4\ (\text{S2})$$

$$\textbf{class II } N_{Bhabha} = 4.4\ \pm 2.5\ (\text{S1})\ \pm 0.7\ (\text{S2})\ \pm 1.9\ (\text{S3})$$

where S1 is the statistical error combined with the systematic one related to the definition of the Bhabha tag, S2 is the systematic related to the misidentification e/π and S3 is the systematic related to the ECAL energy cut in Class II .

7.5 Purity of the $\tau^+\tau^-$ sample

Bhabha background

As described in the previous subsection, the number of Bhabha events surviving in the $\tau^+\tau^-$ sample is $14.1\ ^{+7.6}_{-6.5}$, corresponding to a contamination of $C^{Bhabha} = (2.3^{+1.2}_{-1.1})10^{-3}$. The forward backward asymmetry for this background is dependent on $\sqrt{s}$, as shown in figure 30 (Bhabha selected with the tag defined in the previous subsection), and the values are reported in TABLE III.

μ pair background

This background is measured directly from the data. The missing mass squared distribution of the events in the $\tau^+\tau^-$ sample and with ECAL energy $<0.3\sqrt{s}$ is shown in figure 31, together with the expected distribution for $\tau^+\tau^-$ Monte Carlo. An excess of 95 $\pm$21 events is observed in region $|MM^2| < 400$. The contamination is therefore $C^{\mu^+\mu^-} =$ (1.6 $\pm$0.4)%

2-photon background

From the distribution of the TPC energy, when the ECAL energy is small, and comparing data and $\tau^+\tau^-$ M.C. expectation, an excess of 68 $\pm$18 events is observed in the low energy TPC region. That gives a contamination of $C^{\gamma\gamma} = (1.1 \pm 0.3)\%$

hadronic background

76 000 LUND Monte Carlo events have been processed through GALEPH and JULIA. Only 9 events survive the $\tau^+\tau^-$ selection. This number corresponds to a contamination of $C^{hadronic} = (2.5 \pm 0.8)10^{-3}$, sufficiently small to be neglected.

7.6 Extraction of Afb and background corrections

The data of 1989 and 1990 are grouped in 10 bins in $\sqrt{s}$. For 2 bins, the numbers of events are too small to be used (namely the $\sqrt{s}$ = 92.6 and 95.3 GeV). The center of mass scattering angle θ^* is inferred from the two polar angles of the two τ jets.

For each bin in $\sqrt{s}$, a maximum likelihood is performed on $\cos\theta^*$ fitting the following form:

$$1/NdN/dcos\theta^* = 1 + cos^2\theta^* + \frac{8}{3}A_{FB}cos\theta^* \tag{3}$$

The result does not depend on the acceptance on $\cos\theta^*$, except if the aceptance is $\cos\theta$ and charge dependent. Figures 32 and 33 show the distributions 1/N dN/d$\cos\theta^*$ for two $\sqrt{s}$, 91.2 GeV and 91.5 GeV. The overlaid functions are the results of the fits. Because of the background remaining in the final sample, the fitted value of the Afb, must be corrected for.

The correction for a given type of background depends on the Afb of this background. In the 2 bin approximation, sufficient to estimate the correction from a small background contamination, can be written as follows:

$$Afb^{corr.}(\sqrt{s}) = \frac{Afb^{fit}(\sqrt{s}) - \sum Afb^{bkg}(\sqrt{s}) * C^{bkg}(\sqrt{s})}{1. - \sum C^{backg}(\sqrt{s})} \tag{4}$$

Where, $C^{backg}(\sqrt{s})$ and Afb^{bkg} are respectively the contamination at the center of mass $\sqrt{s}$, and the charge forward backward asymmetry for the residual background of a specific type. Afb^{fit} is the result of the maximum likelihood fit. For the measurement of the Afb in the $\tau^+\tau^-$ channel, the $\mu^+\mu^-$ and hadronic background can be neglected. The Bhabha background is important for the asymmetry. Table III shows the contamination for each $\sqrt{s}$ of data taking, and the Afb of the Bhabha, and the correction to the Afb of the $\tau^+\tau^-$ due to the Bhabha background.

$\sqrt{s}$ (GeV)	C_{Bhabha} %	Afb Bhabha %	δAfb %
88.28	$0.68\ ^{+0.42}_{-0.33}$	65. $\pm$4.2	$-0.44\ \pm0.2$
89.28	$0.43\ ^{+0.28}_{-0.20}$	60. $\pm$4.3	$-0.26\ \pm0.1$
90.28	$0.29\ ^{+0.18}_{-0.14}$	39. $\pm$3.2	$-0.11\ \pm0.1$
91.00	$0.24\ ^{+0.14}_{-0.11}$	32. $\pm$5.7	$-0.08\ \pm0.0$
91.28	$0.20\ ^{+0.13}_{-0.10}$	27. $\pm$1.3	$-0.05\ \pm0.0$
91.50	$0.19\ ^{+0.12}_{-0.10}$	22. $\pm$5.9	$-0.04\ \pm0.0$
92.28	$0.19\ ^{+0.12}_{-0.10}$	29. $\pm$3.8	$-0.05\ \pm0.0$
93.28	$0.20\ ^{+0.13}_{-0.10}$	44. $\pm$4.8	$-0.09\ \pm0.0$
94.28	$0.28\ ^{+0.16}_{-0.12}$	48. $\pm$4.9	$-0.13\ \pm0.1$

Table III
Contaminations as a function of $\sqrt{s}$ for the Bhabha background

Table IV shows the contaminations due to $\gamma\gamma$ background , as a function of $\sqrt{s}$.

$\sqrt{s}$ (GeV)	$C_{\gamma\gamma}$ %
88.28	4.8 ±1.2
89.28	2.6 ±0.7
90.28	1.0 ±0.3
91.00	0.7 ±0.2
91.28	0.7 ±0.2
91.50	0.7 ±0.2
92.28	1.0 ±0.3
93.28	2.0 ±0.5
94.28	2.9 ±0.8

Table IV
Contaminations as a function of $\sqrt{s}$ for the $\gamma\gamma$ background

The final $\tau^+\tau^-$ sample contains 6095 events, for a total of 192 ±28 background events. Table V summarizes the results, with the numbers of selected events, the fitted values of Afb, and the corrected ones. Finally, figure 27 shows the Afb for each $\sqrt{s}$ of the data taken, and the curve is the result of the fit of gv and ga (see 8.7).

$\sqrt{s}$ (GeV)	events	Afb fitted %	Afb cor. %
88.28	92	−35.1 ±9.7	−37.3 ±9.7 ±0.6
89.28	179	−14.8 ±7.6	−15.5 ±7.6 ±0.2
90.28	368	−7.0 ±5.6	−7.2±5.6 ±0.1
91.00	157	−4.8 ±8.2	−4.9 ±8.2 ±0.1
91.28	4127	+2.1 ±1.6	+2.1 ±1.6 ±0.0
91.50	169	+1.8 ±7.9	+1.8 ±7.9 ±0.0
92.28	514	+14.0 ±4.5	+14.1 ±4.5 ±0.1
93.28	284	+27.6 ±5.7	+28.1 ±5.7 ±0.1
94.28	205	+26.2 ±7.0	+26.8 ±7.0 ±0.2

Table V
Summary of the results as a function of $\sqrt{s}$

7.7 Summary and fit result for the ECAL selection

The forward backward asymmetry for Z decays to $\tau^+\tau^-$ has been measured. The sample is selected by μ and π identification. The selection is done in such a way that the Bhabha background is measured from the data as well as the related systematics. The level of the Bhabha contamination is of the order of 2 10^{-3}. The lepton couplings gv and ga are fitted on the variation of the Afb as a function of $\sqrt{s}$. The values of gv and ga are in good agreement with the prediction of the standard model.

The lepton couplings gv and ga are fitted on the Afb and the lepton partial width. To perform the fit, the Afb of the lepton is calculated ,including radiative corrections, by the

program ZBIZON [5]. Figure 27 shows the fitted function (curve) and the data points. The following values are obtained :

sample	events	gv	ga	$\sin^2\theta_W$
$\tau^+\tau^-$	6095	-0.0597 ± 0.010	-0.4957 ± 0.0024	0.220 ± 0.005
$\tau^+\tau^-$,$\mu^+\mu^-$ common sample	13878	-0.0446 ± 0.0080	-0.4972 ± 0.0022	0.2276 ± 0.0040

Table VII
Result of the fits of gv and ga

8 Selection using the missing mass and the HCAL

8.1 Event selection

The two cuts used in the cross section analysis [2] :

- Missing mass > 400 GeV^2
- $E_{ECAL} < 55\%\sqrt{s}$

leave an e^+e^- background under the selected $\tau^+\tau^-$ pairs of $1.1\% \pm 0.5\%$. To further reduce this, it is required, for events with two tracks (1/1 topology):

- the presence of at least one μ in the event
- the presence of at least one HCAL cluster associated with one of the two charged tracks

The μ is identified by requiring 2 out of the last 10 HCAL planes to have fired, or the Julia identification flag to be set (successful comparison between expected and observed pattern) or the presence of a hit in the μ-chambers.

The Hcal cluster may still be due to an electron

- either from leakage from the back of the ECAL
- or because the electron has gone through a crack of the ECAL

In order to avoid longitudinal leakage, the HCAL cluster is required to be penetrating. The digital information is used. One has to remember that: in the barrel ($\theta > 40°$) the first tube layer is in front of the first iron slab. In the end-cap the first iron slab precedes the first tube. The HCAL end-cap starts at plane ♯9 in the angular range $33.7°(29.5°) < \theta < 40°$. (fig. 6) An electron that has showered in the ECAL leaks very little in the HCAL. But if the electron has gone through an ECAL crack it can produce a deep shower in the HCAL. Fig. 4 shows the expected distribution of last versus first HCAL planes hit by electrons from e^+e^- Monte Carlo.

Most of the electron showers starting at plane 1 or 9 (overlap) and going deep in the HCAL are due to electrons having gone through an ECAL crack. This is shown in fig. 5 which shows the same distribution for electrons outside ECAL cracks.

We require that:

- either the shower starts late (the 1st hit plane has to be $\geq plane♯2$)
- or the shower is long (at least 2 tube planes hit)

In order to cross-check the digital information, some energy is required in the Hcal tower associated to the cluster: $E_{tower} > 300MeV$ (threshold).

In order to avoid electrons going through cracks of the ECAL, the HCAL cluster must correspond to a charged track which crosses the ECAL far from the cracks and overlaps. This condition rejects also electrons which emitted a γ going through an ECAL crack: the cluster in this case does not correspond to a charged track (fig. 7)

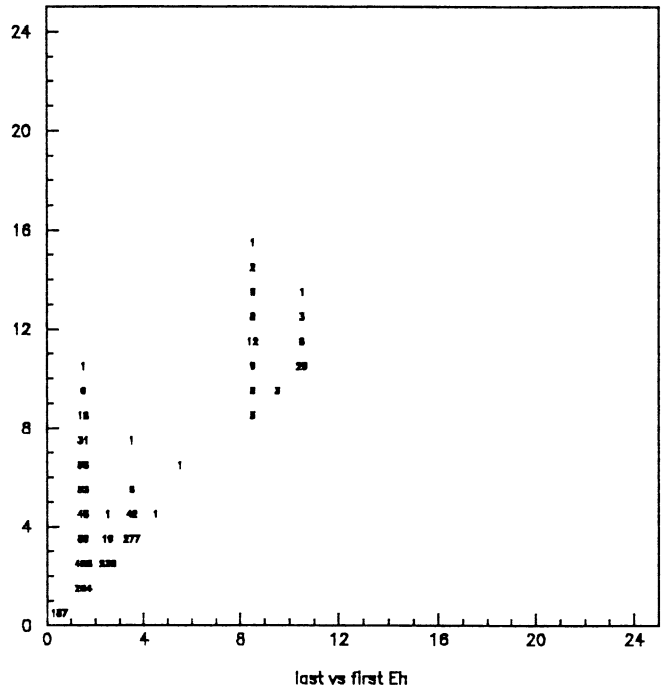

Figure 4: Last versus first HCAL plane hit by MC electrons (from e^+e^- MC)

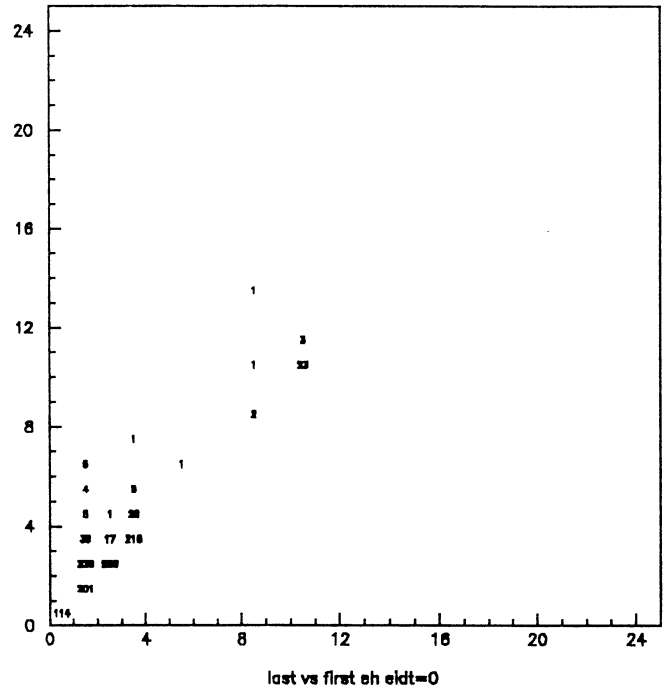

Figure 5: Last versus first HCAL plane hit by MC electrons outside ECAL cracks

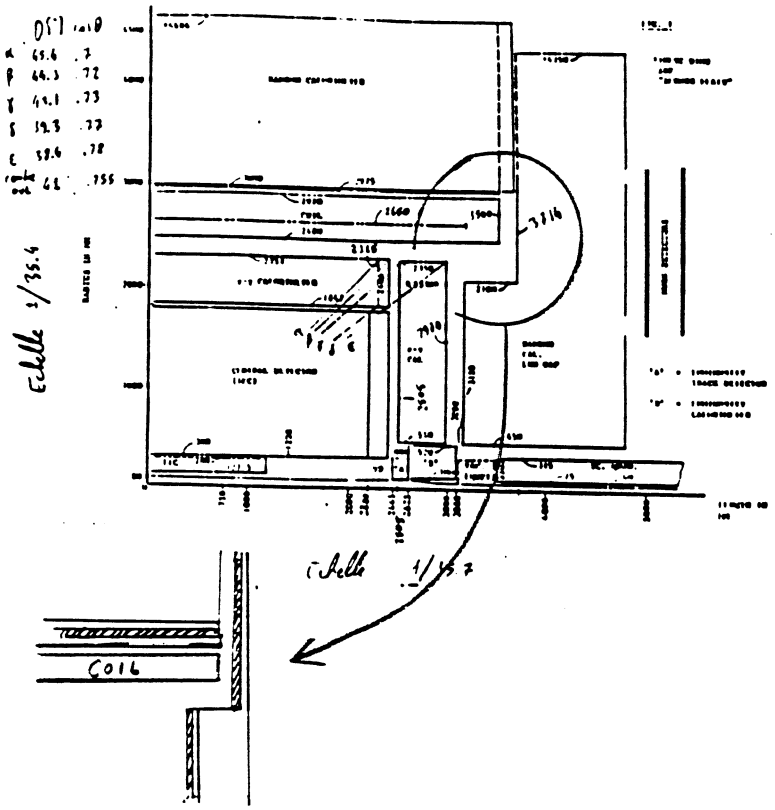

Figure 6: Detail of the HCAL structure

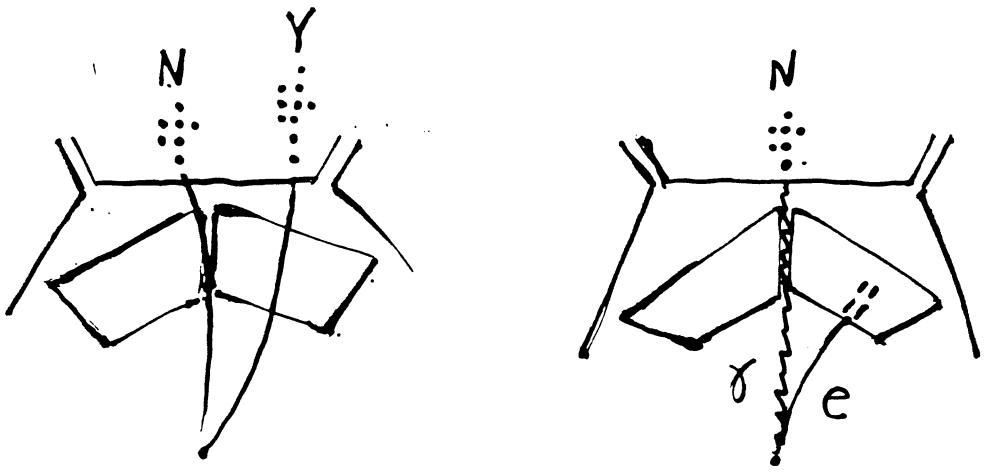

Figure 7: Selection of charged tracks associated to an Hcal cluster : Y = selected, N = not selected

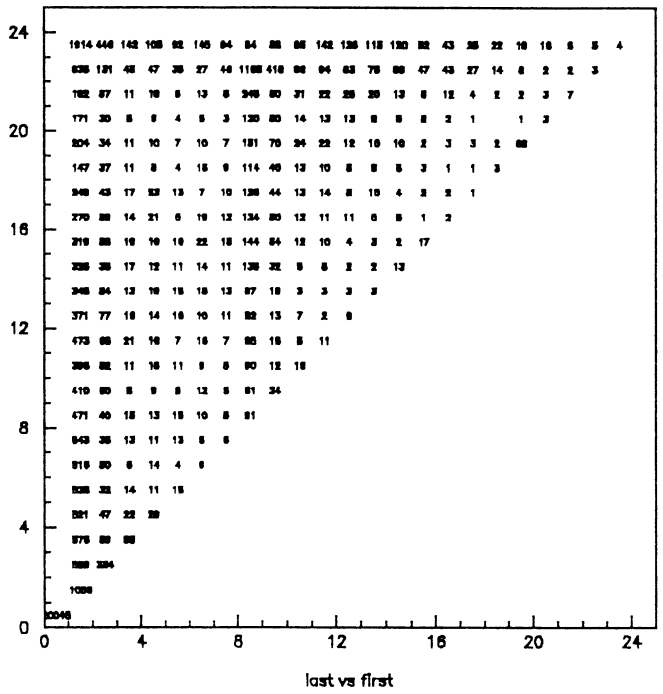

Figure 8: Last versus first HCAL plane hit for class 15 events

8.2 e^+e^- background

The reduction expected from MC of e^+e^- events using the cuts described above is 3.3 $\pm$ 0.07 in the Barrel and 3.2 $\pm$ 0.1 in the End Caps.

In order to confirm this reduction factor from the data, a sample of events with at least one identified electron was used. The penetration in the Hcal was then measured on the opposite side.

We start with a sample of class 15 events. Fig. 8 shows the distribution of last versus first HCAL planes hit.

Then we ask for events with a clear electron identified on one side in the ECAL and look at the track on the opposite side. This track has to enter the ECAL outside cracks. (Fig. 9)

Fig. 10 shows the distribution of last versus first HCAL planes hit by the opposite side track if it has deposited at least 200 MeV in the HCAL.

Fig. 11 shows the distribution of the energy deposited in the HCAL (data and MC)

Electron leakage in the HCAL seems to be well described by the MC for the purpose of this analysis. The reduction factor found on data is 3.3, like in MC. The resulting average contamination is 0.3% $\pm$ .05% . On events with high missing mass, using MC, the rejection was found to be less strong: 2.8 $\pm$ 0.8 in the Barrel and 1.7 $\pm$ 0.3 in the End Caps. The e^+e^- contamination for each energy point is shown in table 3.

The effect on A_{FB}^{τ} was computed using Alibaba. At each energy point, e^+e^- A_{FB} was computed separately for the Barrel and the EC, as shown in table 4. The resulting corrections and systematic errors on A_{FB}^{τ} are shown in table 3.

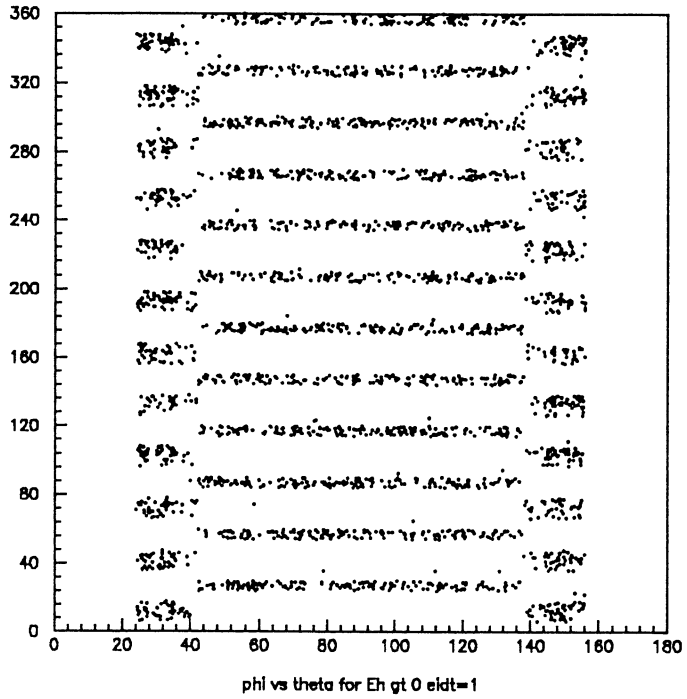

Figure 9: ϕ vs θ at ECAL entry of rejected tracks crossing cracks in data Class 15 events

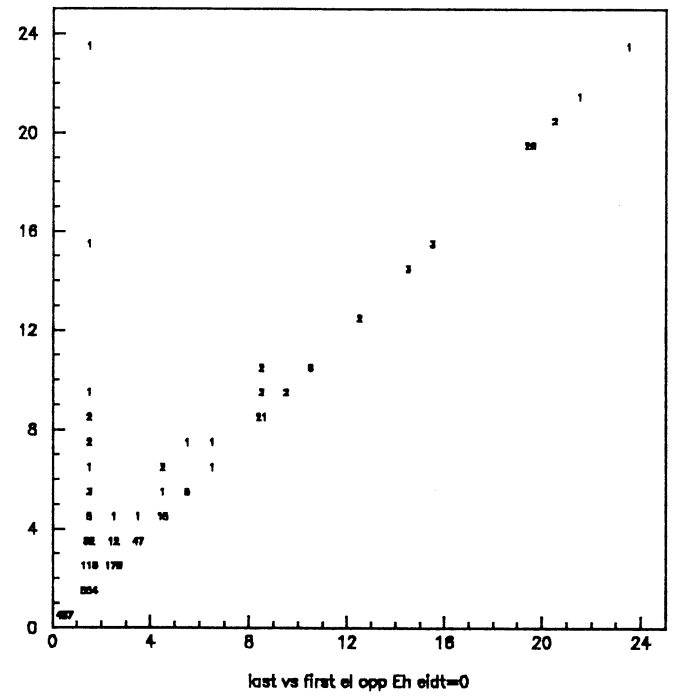

Figure 10: Last versus first HCAL plane hit for tracks opposite from an identified electron and outside ECAL cracks (data)

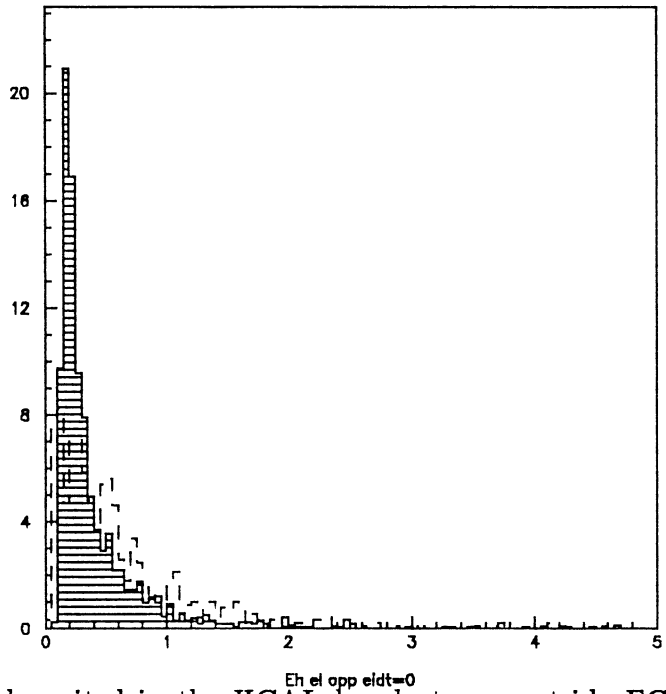

Figure 11: Energy deposited in the HCAL by electrons outside ECAL cracks for data (shaded histogram) and MC

Table 3: Backgrounds and A^{τ}_{FB} corrections for HCAL selection

$\sqrt{s}$ (GeV)	$C^{\gamma\gamma}$ (%)	$\delta A_{\gamma\gamma}$ (%)	$C^{q\bar{q}}$ (%)	$\delta A_{q\bar{q}}$ (%)	$C^{Bhab.}$ (%)	$\delta A_{Bhab.}$ (%)
88.23	3.1±1.3	−1.17±0.5	1.3±0.4	−0.49±0.16	1.6±0.7	−2.0 ±0.8
89.23	3.2±0.6	−0.57±0.1	1.4±0.4	−0.25±0.07	1.1±0.4	−1.0 ±0.4
90.23	1.4±0.3	−0.11±0.02	1.4±0.4	−0.1±0.03	0.7±0.2	−0.55 ±0.18
91.03	0.8±0.2	0.02±0.006	1.4±0.4	0.04±0.01	0.6±0.2	−0.3 ±0.12
91.22	0.8±0.2	0.01±0.004	1.4±0.4	0.03±0.007	0.47±0.09	−0.22 ±0.05
91.53	0.8±0.2	0.01±0.001	1.4±0.4	0.01±0.003	0.7±0.2	−0.34 ±0.13
92.23	1.2±0.2	0.14±0.025	1.1±0.3	0.14±0.04	0.55±0.17	−0.16 ±0.07
93.23	2.3±0.4	0.55±0.1	1.7±0.5	0.4±0.1	0.8±0.3	−.28 ±0.13
94.23	3.1±0.6	0.77±0.16	1.3±0.4	0.3±0.09	0.8±0.3	−.28 ±0.15

Table 4: e^+e^- A_{FB} computed with Alibaba

$\sqrt{s}$ (GeV)	A_{FB} Barel %	A_{FB} EC %
88.23	40	89
89.23	31	85
90.23	20	74
91.23	11	59
92.23	7.5	61
93.23	11	72
94.23	17	81

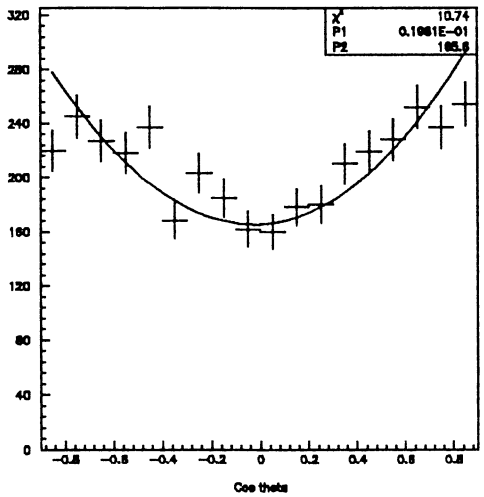

Figure 12: cos θ^* distribution at the pole

Table 5: A^{τ}_{FB} from HCAL selection

$\sqrt{s}$ (GeV)	Events	A^{obs}_{fb} (%)	ΔA_{fb} (%)	A^{corr}_{fb} (%)
88.23	84	-35.7 ± 9.7	-3.6 ± 1.0	$-39.3 \pm9.7 \pm1.0$
89.23	152	-16.7 ± 8.0	-1.8 ± 0.4	$-18.5 \pm8.0 \pm0.4$
90.23	368	-7.0 ± 5.3	-0.75 ± 0.18	$-7.80 \pm5.3 \pm0.18$
91.03	148	$+3.4\pm8.0$	-0.23 ± 0.12	$+3.2 \pm8.0 \pm0.12$
91.22	3783	$+2.0\pm1.6$	-0.18 ± 0.05	$+1.8 \pm1.6 \pm0.05$
91.53	146	$+1.0\pm8.2$	-0.33 ± 0.13	$+0.70 \pm8.2 \pm0.13$
92.23	483	$+12.2\pm4.5$	$+0.12\pm0.09$	$+12.3 \pm4.5 \pm0.09$
93.23	260	$+24.0\pm5.7$	$+0.67\pm0.20$	$+24.7 \pm5.7 \pm0.2$
94.23	184	$+25.0\pm7.2$	$+0.81\pm0.23$	$+25.8 \pm7.2 \pm0.23$

8.3 $\gamma\gamma$ and $q\bar{q}$ background

These backgrounds are those of the missing mass selection (see [2] and Section 7). The resulting corrections and systematic errors on A^{τ}_{FB} for this selection are shown in table 3.

8.4 Charge configurations

The charges of the 2 τ 's have to be known without ambiguity in order to measure A_{FB} . Events with opposite charges in the two hemispheres are kept. Figure 13 shows the observed charge configurations of selected events. Comparing configurations -1/+1 to

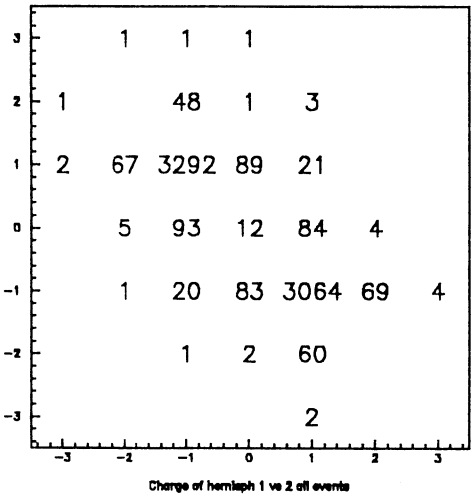

Figure 13: Charge 2 vs charge 1 for all selected $\tau^+\tau^-$ events

-1/-1, we deduce that the probability of wrong sign assignment is $\simeq$ 0.6 % per side. Thus configurations +1/-1 have no risk of confusion ($(0.6\%)^2$) The probabilities +1 $\rightarrow$ -2 and -2 $\rightarrow$ +1 are smaller, so the configurations +1/-2 and -1/+2 have no risk of confusion either. The other cases are rejected.

8.5 Fits to the angular distributions of the HCAL selection

Fig. 12 shows the angular distribution of the $\tau^+\tau^-$ events, at the peak, as a function of θ^*, the centre-of-mass scattering angle between the incoming e^- and the outgoing fermion, defined as:

$$\cos\theta^* = \cos\frac{1}{2}(\theta_1 + \pi - \theta_2) \;/\; \cos\frac{1}{2}(\theta_1 - \pi + \theta_2), \tag{5}$$

where θ_1 and θ_2 are the polar angles of the vector sum of the track momenta in each hemisphere corresponding respectively to the outgoing fermion and anti-fermion. This variable preserves the true angular distribution in the e^+e^- centre-of-mass when hard collinear radiation takes place from the initial state.

The τ direction and charge are defined as the sum of momenta and the sum of the charges of the charged particles in its decay jet. Using KORALZ to measure the difference between the real and the reconstructed τ direction, one finds a dispersion of 30 mrad, which is negligible for the asymmetry measurement.

Events are studied in the angular region $|\cos\theta^*| < 0.9$.

In order to extract the forward-backward asymmetry, $A_{\rm FB}$, the angular distribution at each centre-of-mass energy is fitted by the function

$$\frac{\mathrm{d}\sigma}{\mathrm{d}\cos\theta^*} = C \cdot (1 + \cos^2\theta^* + \frac{8}{3} A_{\rm FB}\ \cos\theta^*) \tag{6}$$

using a maximum likelihood method. Here C is a normalization constant. The corrected asymmetry over the whole range $|\cos\theta^*| < 1$ is computed from Eq. (6). I has been shown that if the acceptance is charge-and-F/B symmetric, it doesn't affect the result.

In Table 5 the forward-backward asymmetry is listed for the different centre-of-mass energies.

8.6 Fit to the Energy - Asymmetry plot

At Born level the asymmetry is given by:

$$A^0_{FB} = \frac{3}{4} \frac{2Q_eQ_fa_ea_fRe\ \chi_0(s) + 4v_ea_ev_fa_f \mid \chi_0(s) \mid^2}{Q_e^2Q_f^2 + 2Q_eQ_fv_ev_fRe\ \chi_0(s) + (v_e^2+a_e^2)(v_f^2+a_f^2) \mid \chi_0(s) \mid^2}$$

We can use, equivalently,

$$g_{V\ell} = -\frac{1}{2} + 2\sin^2\theta_w \quad , \quad g_{A\ell} = -\frac{1}{2}$$

Non-photonic corrections are taken into account using the "improved Born approximation" which includes the bulk of the $O(\alpha)$ electroweak corrections. The coupling constants become "running". Their numerical values refer to $Q^2 = M_Z^2$ and depend on the masses of the top quark and of the Higgs boson.

At the Z peak the asymmetry is:

$$A_{FB} = 3 \frac{g_{Ve}(M_Z^2)g_{Ae}(M_Z^2)}{g_{Ae}^2(M_Z^2) + g_{Ve}^2(M_Z^2)} \cdot \frac{g_{Vf}(M_Z^2)g_{Af}(M_Z^2)}{g_{Af}^2(M_Z^2) + g_{Vf}^2(M_Z^2)}.$$

Off the peak its variation with s depends mainly on $g_{Ae}(M_Z^2)g_{Af}(M_Z^2)$.

Thus the measurement of A^τ_{FB} gives $g_{Ve}(M_Z^2)g_{V\ell}(M_Z^2)\ /g_{Ae}(M_Z^2)g_{A\ell}(M_Z^2)$, or, assuming lepton universality, $g_{V\ell}^2(M_Z^2)\ /g_{A\ell}^2(M_Z^2)$.

On the other hand, the measurement of the leptonic width $\Gamma_{\ell\ell}$ permits a determination of $g_{V\ell}^2(M_Z^2)\ + g_{A\ell}^2(M_Z^2)$:

$$\Gamma_{\ell\ell} = F\,\alpha(M_Z^2)\,\frac{M_Z}{3}\,(g_{V\ell}^2(M_Z^2) + g_{A\ell}^2(M_Z^2)). \qquad (7)$$

where

$$F = \frac{G_F M_Z^2}{2\sqrt{2}\pi\alpha(M_Z^2)} = 1.406,$$

The fit to the measured asymmetries as a function of $\sqrt{s}$ in order to extract the electroweak parameters was done with a fitting program which was first used by the muon group ([6]).

Higher order electroweak effects have been taken into account in the fit. Non-photonic corrections are included by writing the tree-level asymmetry in terms of effective couplings and s-dependent Γ_Z. Photonic corrections are added by convoluting the non-radiative

forward and backward cross sections with a suitable radiator function ([7]) (But the effective coupling is taken constant for all s).

In the fit the values of M_Z and Γ_Z are used together with the constraint on $g^2_{V\ell}(M_Z^2)$ and $g^2_{A\ell}(M_Z^2)$ from the lepton width, Eq. 7. The latter essentially fixes the value of $g^2_{A\ell}(M_Z^2)$ and its error, since $g^2_{V\ell}(M_Z^2) \ll g^2_{A\ell}(M_Z^2)$. The best result on $g^2_{V\ell}(M_Z^2)$ will come from the combined fit of the 3 leptons. However, to show the significance of $g^2_{V\tau}(M_Z^2)$, we fit here only A^τ_{FB} constrained by $\Gamma_{\ell\ell}$. A two parameter constrained fit to the data yields:

$$g^2_{V\tau}(M_Z^2) = (3.45 \pm 1.13)\ 10^{-3} \quad \text{and} \quad g^2_{A\ell}(M_Z^2) = 0.246 \pm 0.0024$$

with $\chi^2 = 7.4$ for 8 degrees of freedom.

The asymmetries and the fitted curve are shown in Fig. 14.

Figure 14 Measured values of A_{FB} as a function of CM energy The line is the result of a fit to $a_e * a_\tau$, $v_e * v_\tau$ coupling constants .

31−JAN−91 15:26:26

FCN	7.37554
1 v*v	4.84576E−03
	+− 1.59895E−03
2 a*a	0.34771
	+− 3.34457E−03

no. entries = 9

$v^2(M_Z)$ = 0.001495

$a^2(M_Z)$ = 0.349061

M_Z = 91.182

Γ_Z = 2.48800

Γ_{lept} = 0.08330

$\Delta\Gamma_{lept}$ = 0.00070

m_{top} = 150.000

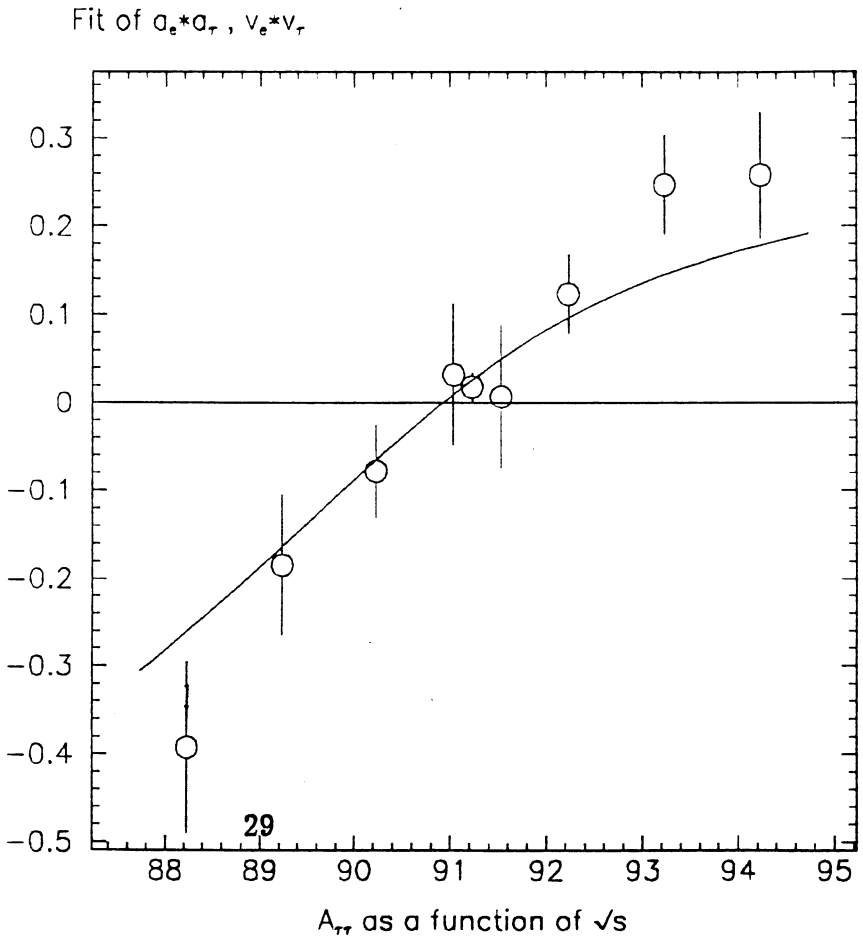

Table 6: Numbers of $Z \to \tau^+\tau^-$ decays, obtained by the three selections. The first column has to be multiplied by an overall factor 1.05 to be compared with the other two.

$\sqrt{s}$ (GeV)	$N_{\tau\tau}$	$N_{\tau\tau}$	$N_{\tau\tau}$
88.23	84	92	84
89.23	170	179	152
90.23	344	368	368
91.03	168	157	148
91.22	3902	4127	3783
91.53	185	169	146
92.23	481	514	483
93.23	264	284	260
94.23	204	205	184

Table 7: A^{τ}_{FB} from the three selections

$\sqrt{s}$ (GeV)	A^{corr}_{fb} (%)	A^{corr}_{fb} (%)	A^{corr}_{fb} (%)
88.23	$-38.8 \pm 9.4 \pm 0.9$	$-37.3 \pm 9.7 \pm 0.6$	$-39.3 \pm 9.7 \pm 1.0$
89.23	$-10.6 \pm 7.5 \pm 0.4$	$-15.5 \pm 7.6 \pm 0.2$	$-18.5 \pm 8.0 \pm 0.4$
90.23	$-5.6 \pm 5.5 \pm 0.3$	$-7.2 \pm 5.6 \pm 0.1$	$-7.8 \pm 5.3 \pm 0.2$
91.03	$+8.2 \pm 7.5 \pm 0.1$	$-4.9 \pm 8.2 \pm 0.1$	$+3.2 \pm 8.0 \pm 0.1$
91.22	$+1.1 \pm 1.6 \pm 0.03$	$+2.1 \pm 1.6 \pm 0.0$	$+1.8 \pm 1.6 \pm 0.05$
91.53	$-3.4 \pm 7.0 \pm 0.1$	$+1.8 \pm 7.9 \pm 0.0$	$+0.7 \pm 8.2 \pm 0.1$
92.23	$+14.7 \pm 4.4 \pm 0.2$	$+14.1 \pm 4.5 \pm 0.1$	$+12.3 \pm 4.5 \pm 0.09$
93.23	$+20.1 \pm 5.7 \pm 0.2$	$+28.1 \pm 5.7 \pm 0.1$	$+24.7 \pm 5.7 \pm 0.2$
94.23	$+22.8 \pm 6.6 \pm 0.4$	$+26.8 \pm 7.0 \pm 0.2$	$+25.8 \pm 7.2 \pm 0.2$

9 Conclusions

In Table 6 the event numbers obtained by the three selections are listed. For a comparison of the selections the numbers for the first selection have to be multiplied by 1.05, essentially because they include only events with +1/-1 configuration (see figure 13)(and because of the higher $\mu^+\mu^-$ background of the second selection).

In Table 7 the forward-backward asymmetries obtained by the three selections are listed.

The three analyses are in agreement. The statistical error is, for the time being, much larger than the systematic one. By careful analysis we can keep the systematics very low, the lowest being achieved by the second analysis. The third analysis has lower efficiency than the first two.

References

[1] Aleph coll/n, D.Decamp et al, Z. Phys. C 48, 365 (1990)

[2] Measurement of the cross section and forward backward asymmetry for the process $e^+e^- \rightarrow \tau^+\tau^-$, G.Apollinari et al [Aleph-note 90-189]

[3] A new selection for large angle Bhabhas, R.Clifft,E.Locci [Aleph-note 90-180]

[4] Charged forward backward asymmetry in Z decays to $\tau^+\tau^-$, J.C. Brient [Aleph-note 91-7]

[5] M. Boehm et al, Z physics at LEP 1, CERN 89-08,Vol 1,203

[6] A.Jahn Aleph notes 89-18, 89-118

[7] S.Jadach and Z.Was, MPI-PAE/PTh 33/ 1989

Figure Captions

15. TPC dE/dx information: number of σ for electron hypothesis versus the number of σ for π hypothesis

16. Mass $\gamma\gamma$ in one hemisphere. The histogram is the distribution for the $\tau^+\tau^-$ sample (data) and the shaded histogram is the distribution for the same data but for the Bhabha tag sample (tagged in the hemisphere opposite to the 2 photons).

17.Percentage of the number of π per hemisphere for Bhabha tag sample, for $\mu^+\mu^-$ and for $\tau^+\tau^-$. In the case of the $\tau^+\tau^-$, the histogram superposed to the data (points with error bars), is the prediction of the KORALZ Monte Carlo $Z \rightarrow \tau^+\tau^-$, after Galeph and Julia.

18-20 Percentage of the number of π per hemisphere for Bhabha tag sample: 18. for ECAL Barrel ($|cos\theta| < 0.6$), 19. for overlap ($0.6 < |cos\theta| < 0.8$), and 20. for ECAL End Cap ($0.8 < |cos\theta| < 0.9$)

21-23 ECAL wires energy normalized to the beam energy, for Bhabha tag event with one pion in event. figure 7 for ECAL barel, 8 for overlap and 9 for End Cap.

24. Distribution of the selected events in the plane Energy TPC versus Energy ECAL (both normalize to $\sqrt{s}$)

25. TPC energy normalized to $\sqrt{s}$, for the selected events when the ECAL energy is less than 5. GeV

26. TPC energy normalized to $\sqrt{s}$, for the selected events when the ECAL energy is larger than 40. GeV

27. Missing mass squared distribution for the selected events when the ECAL energy is larger than 40. GeV

28. ECAL wires energy normalized to $\sqrt{s}$, for selected events, when the TPC energy is larger than $0.5\sqrt{s}$

29. Variation of the misidentification e/π for the Bhabha tag sample as a function of the E^{wires}_{ECAL} / E_{beam}cut for the tag. Each ECAL region is presented separatly.

30. Variation of the Afb for the Bhabha tag sample, as a function of $\sqrt{s}$.

31. Missing mass squared distribution for the final $\tau^+\tau^-$ sample, when Ecal energy $< 0.3\sqrt{s}$

32.-33. For the $\tau^+\tau^-$ final sample, $\frac{1}{N}$dN/dcosθ^* for two points in $\sqrt{s}$. The curve on each figure is the result of the maximum likelihood fit.

34. Variation of the Afb for the $\tau^+\tau^-$ sample, as a function of $\sqrt{s}$. The curve is the fitted function of the fit of gv and ga.

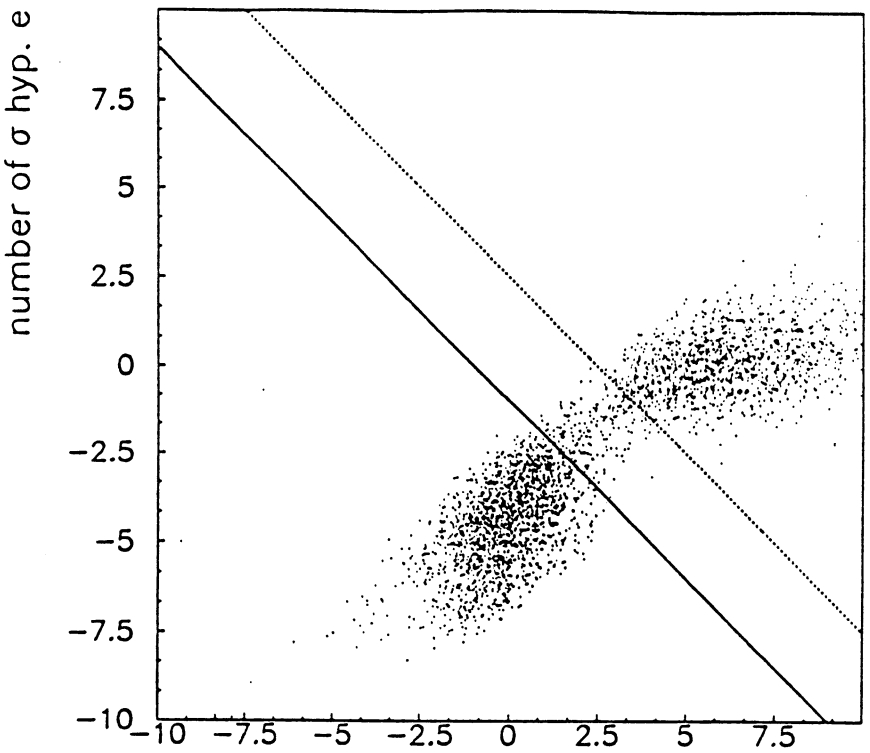

figure 15

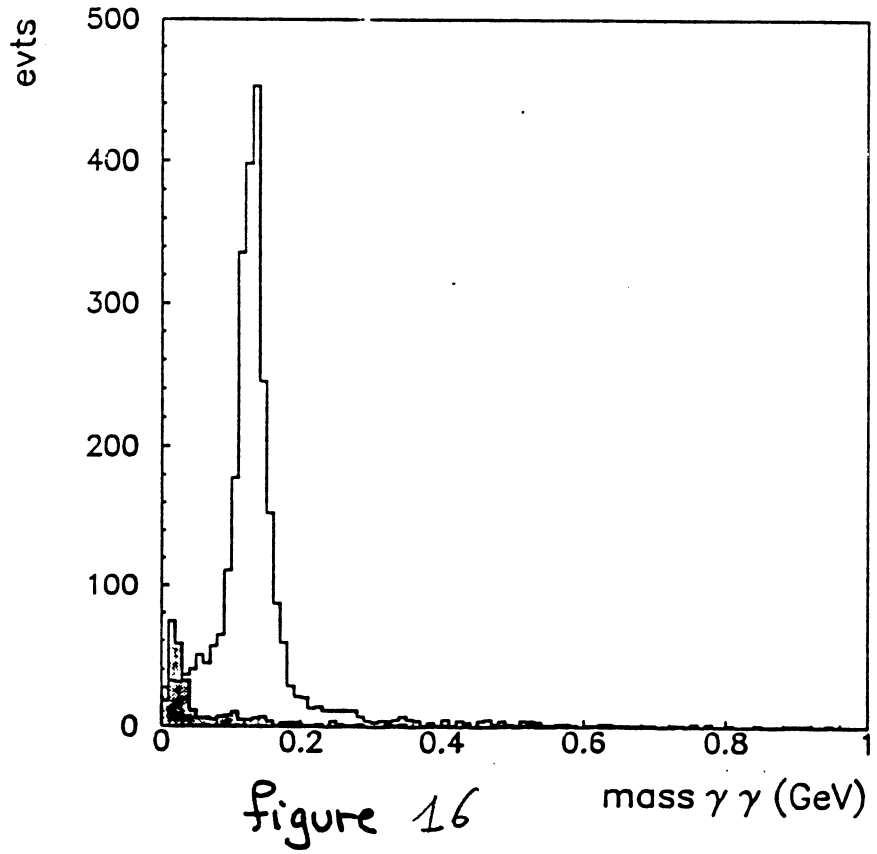

figure 16

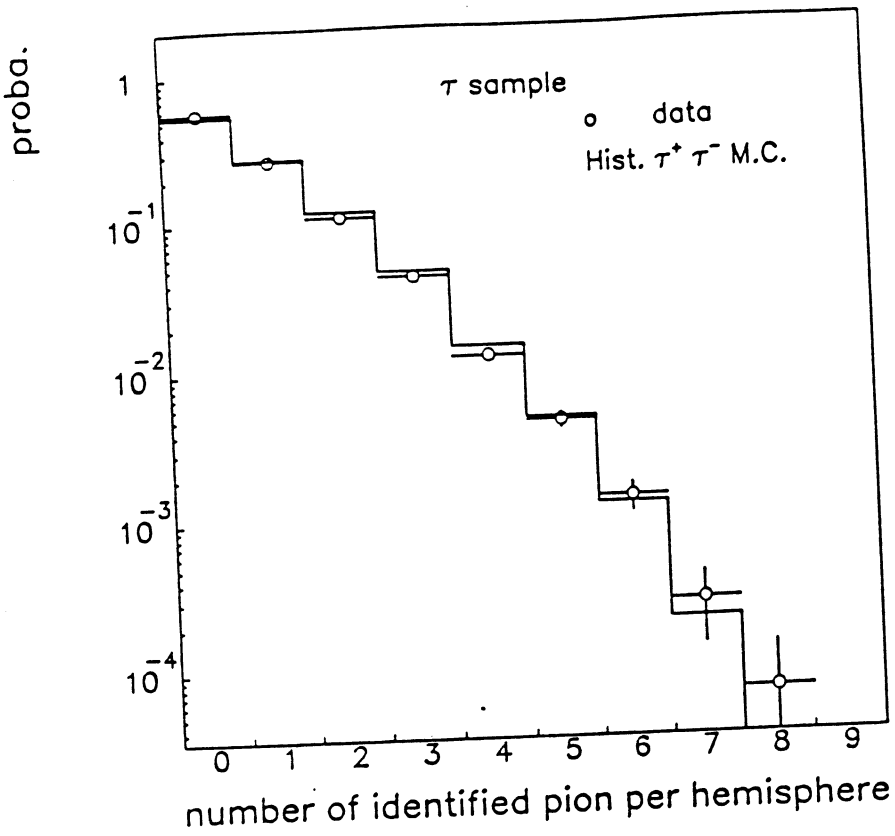
proba.
τ sample
o data
Hist. τ⁺ τ⁻ M.C.
1
10⁻¹
10⁻²
10⁻³
10⁻⁴
0 1 2 3 4 5 6 7 8 9
number of identified pion per hemisphere

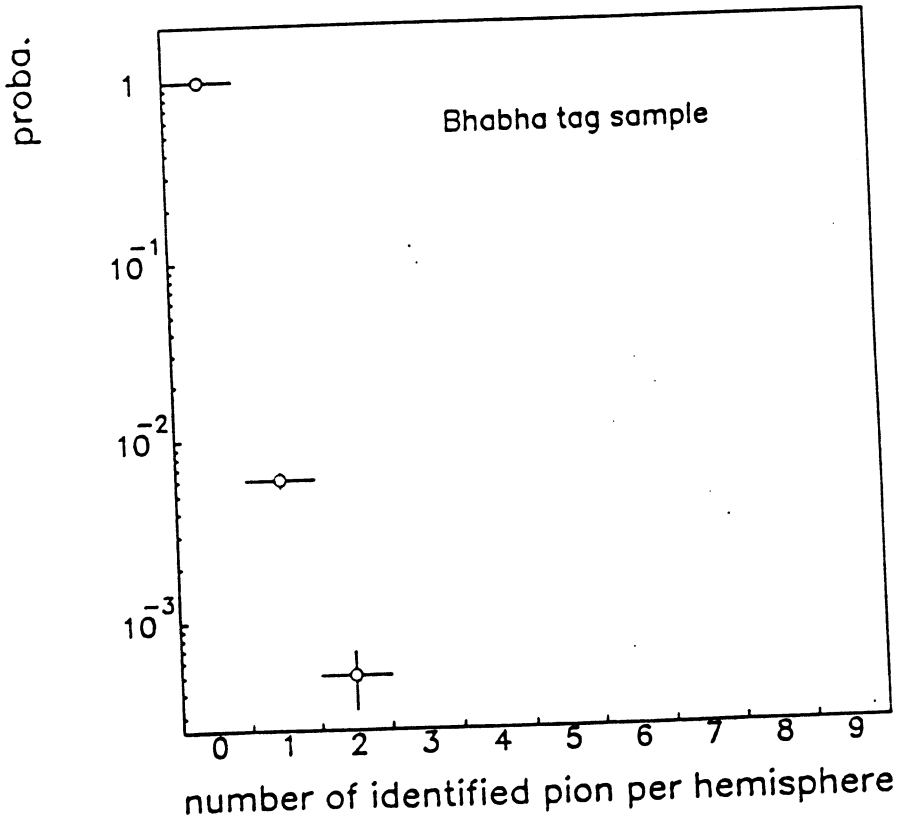
proba.
Bhabha tag sample
1
10⁻¹
10⁻²
10⁻³
0 1 2 3 4 5 6 7 8 9
number of identified pion per hemisphere

figure 17

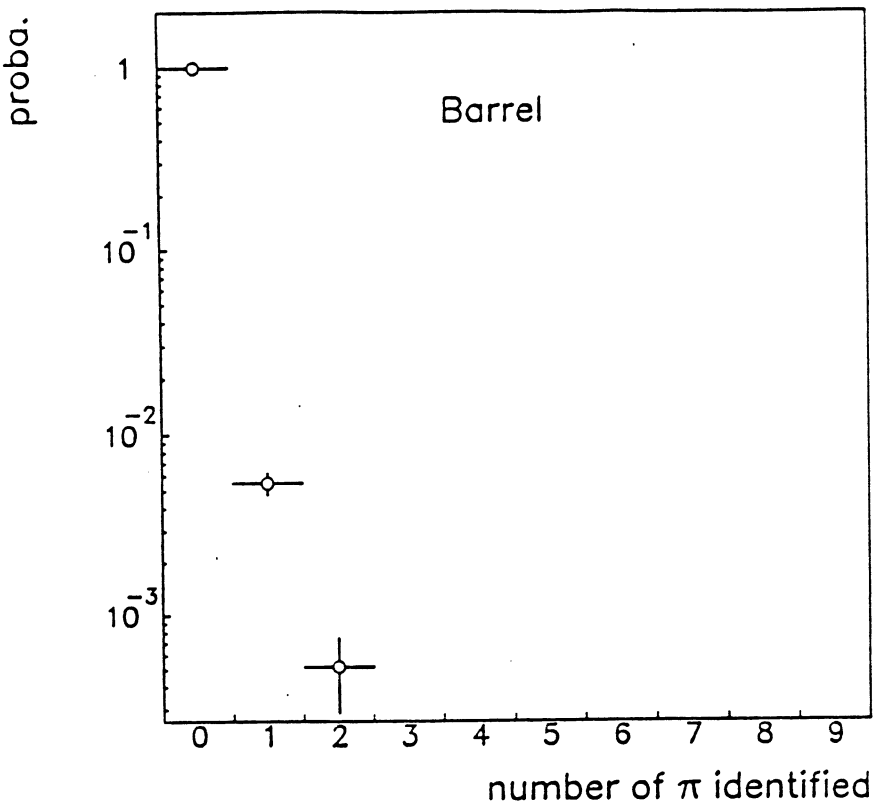

figure 18

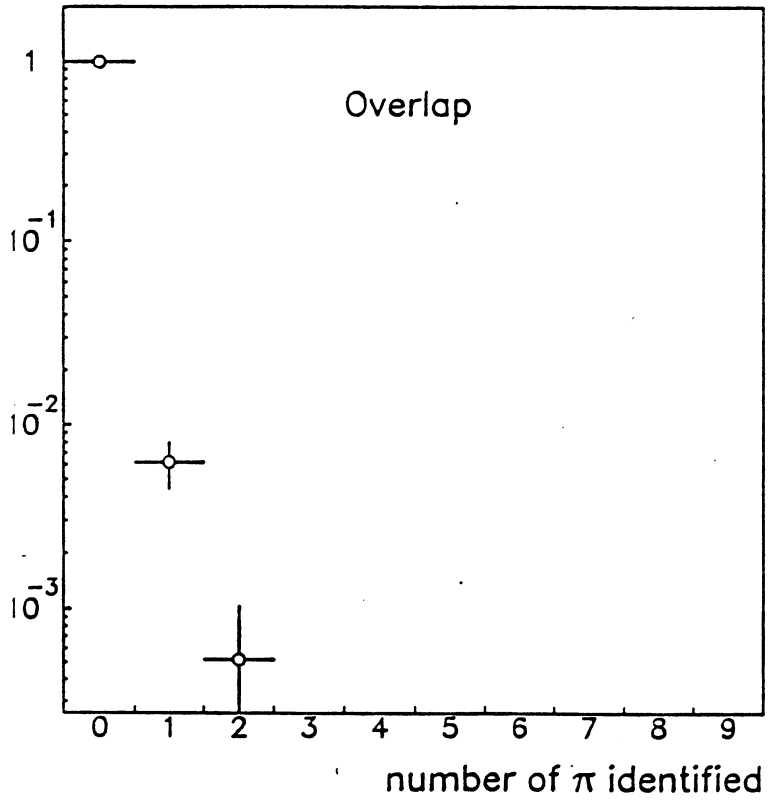

figure 19

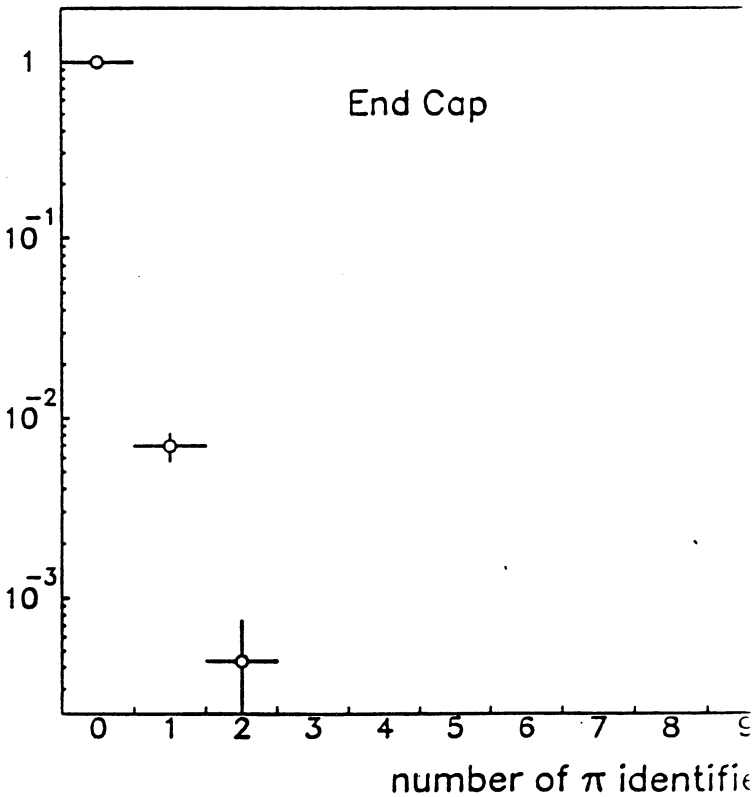

figure 20

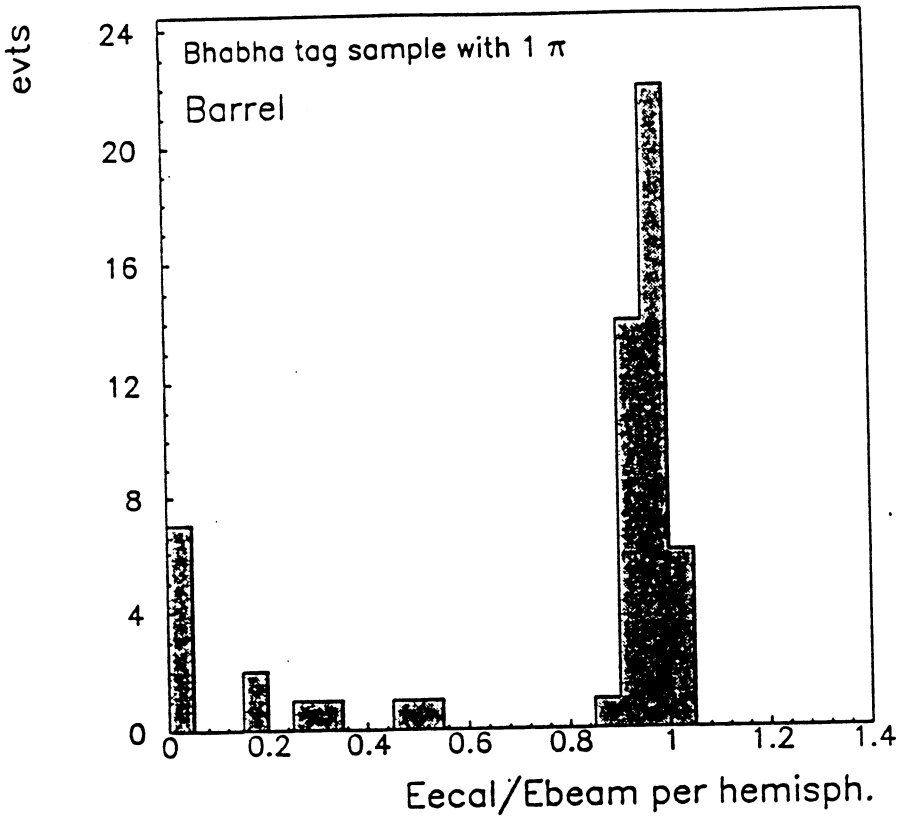

figure 21

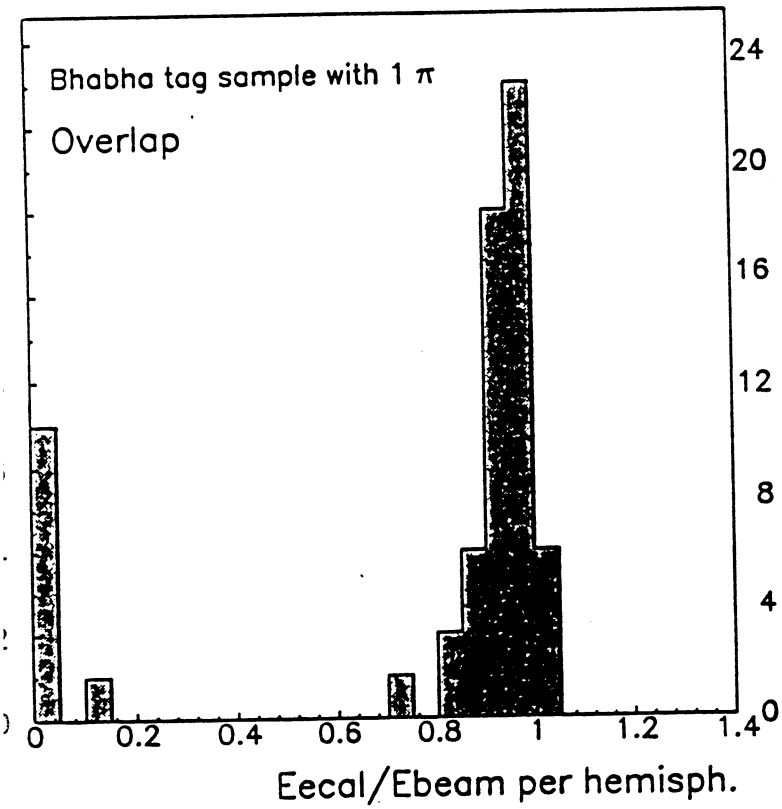

figure 22

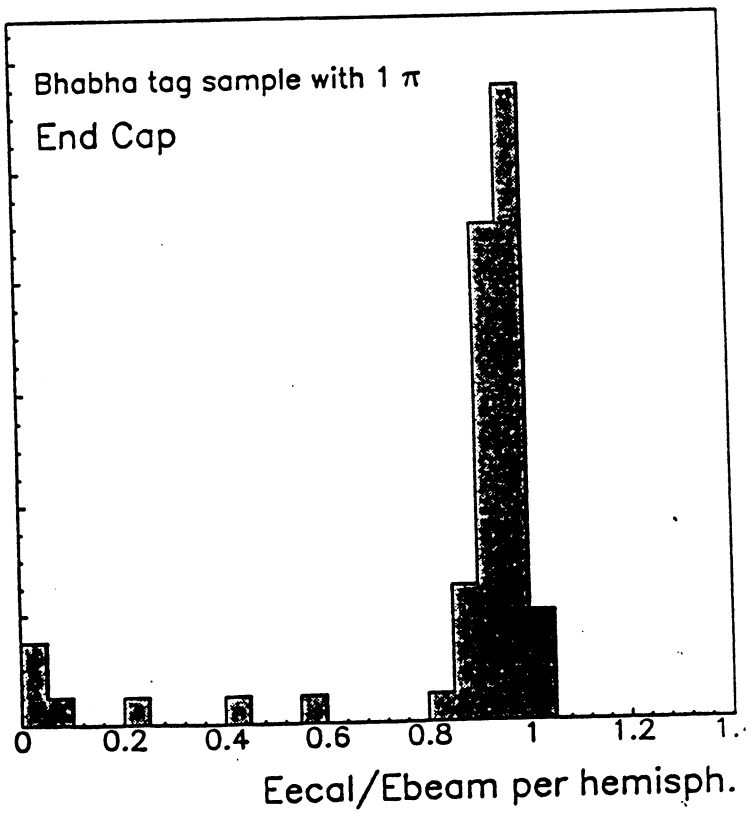

figure 23

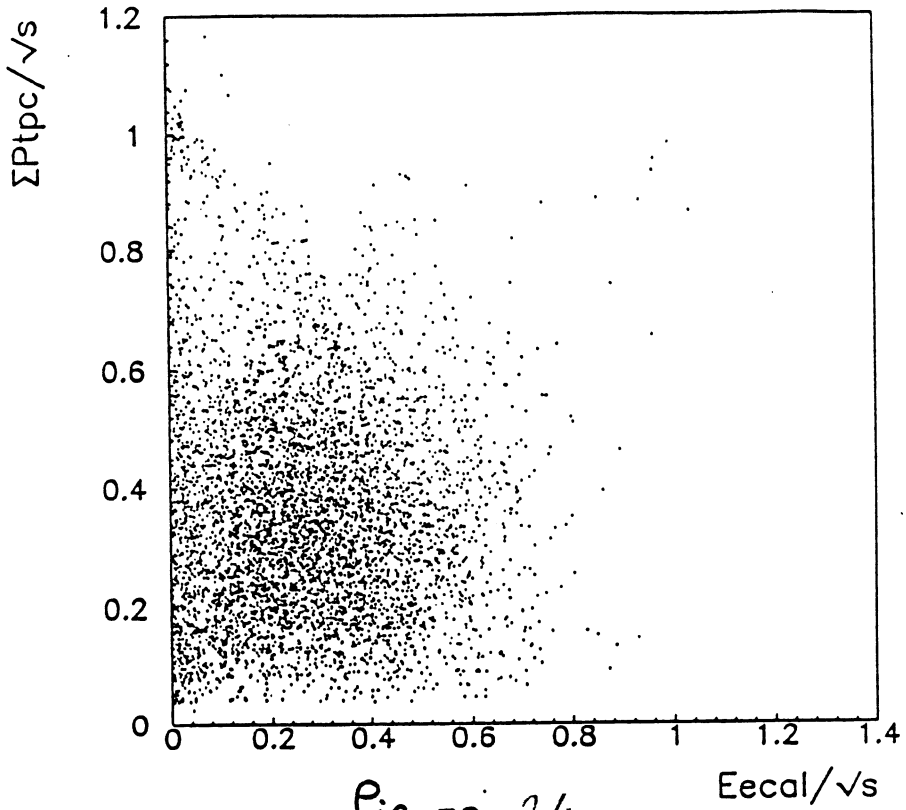

figure 24

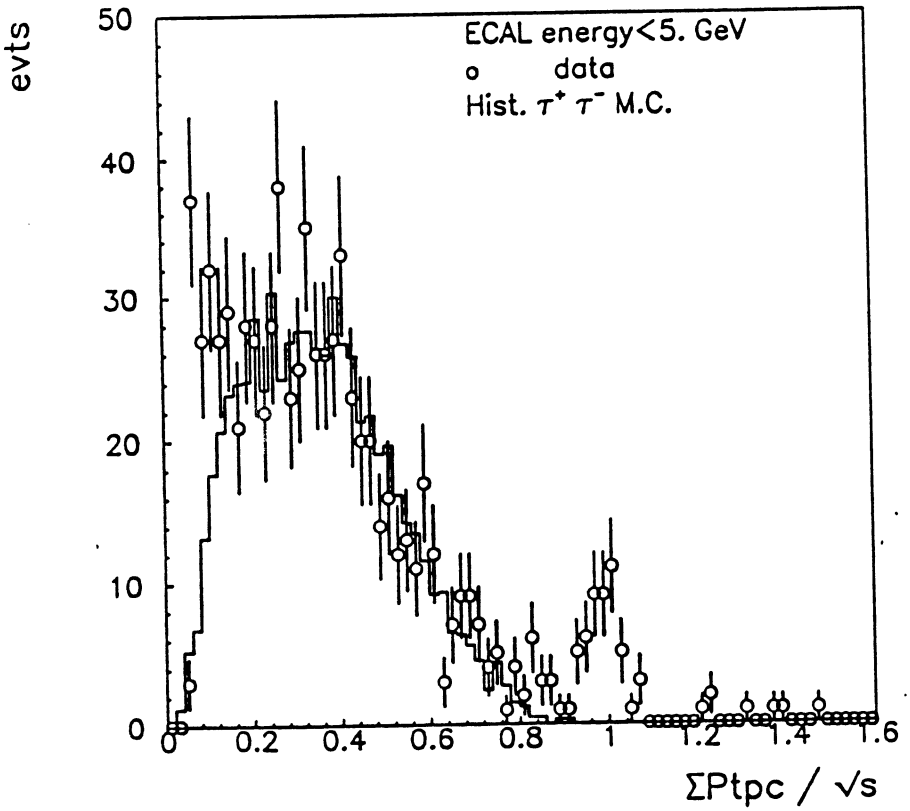

figure 25

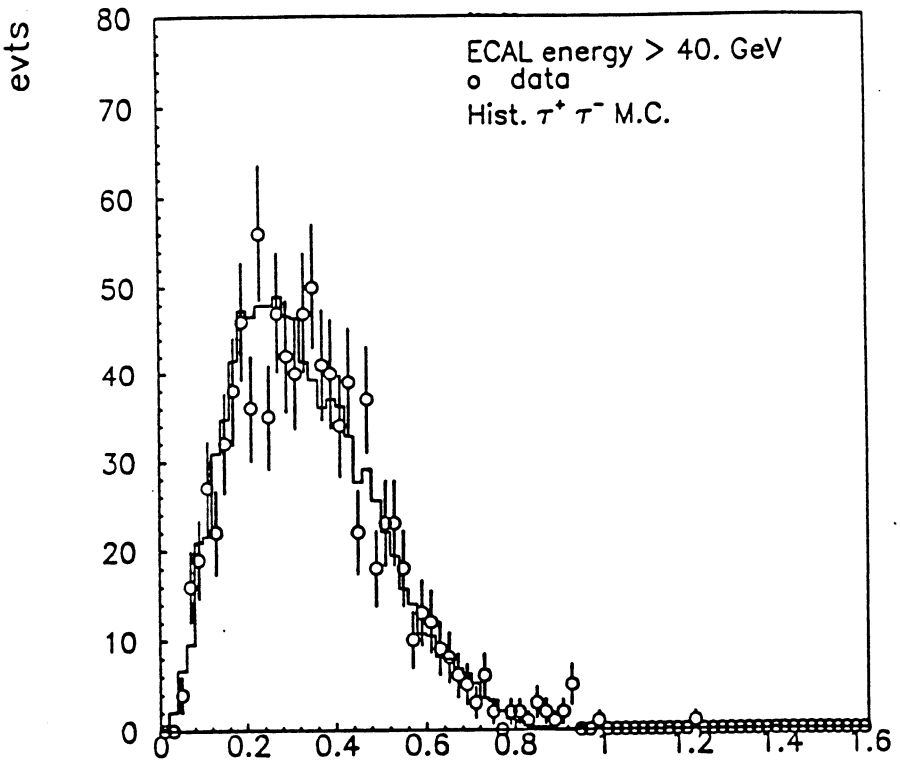

figure 26

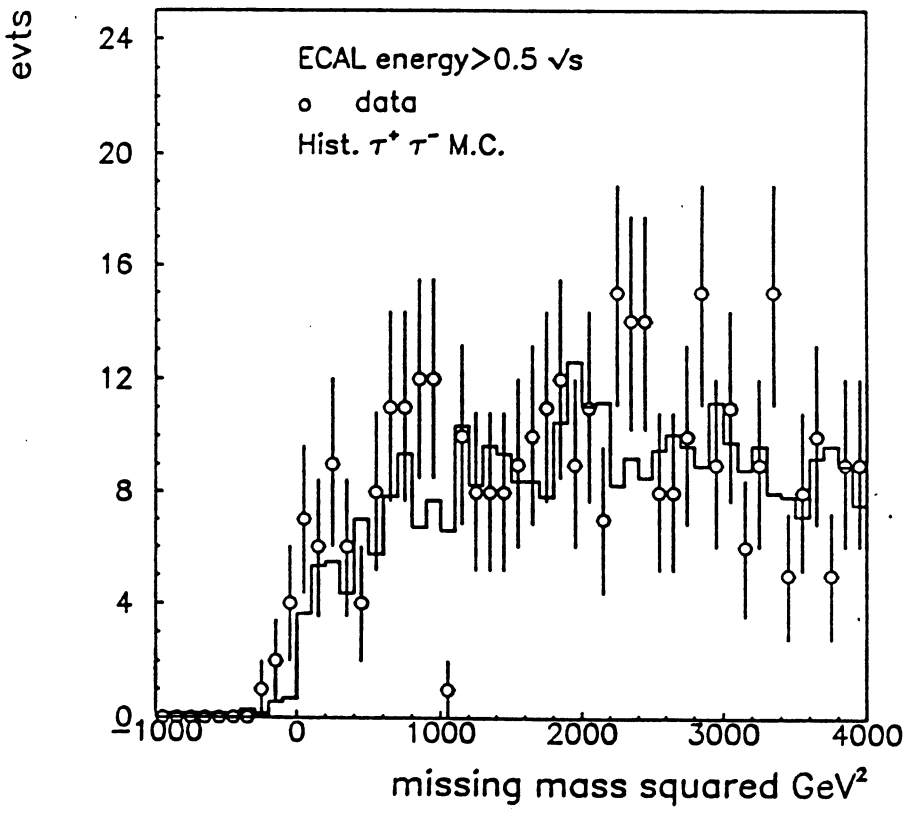

figure 27

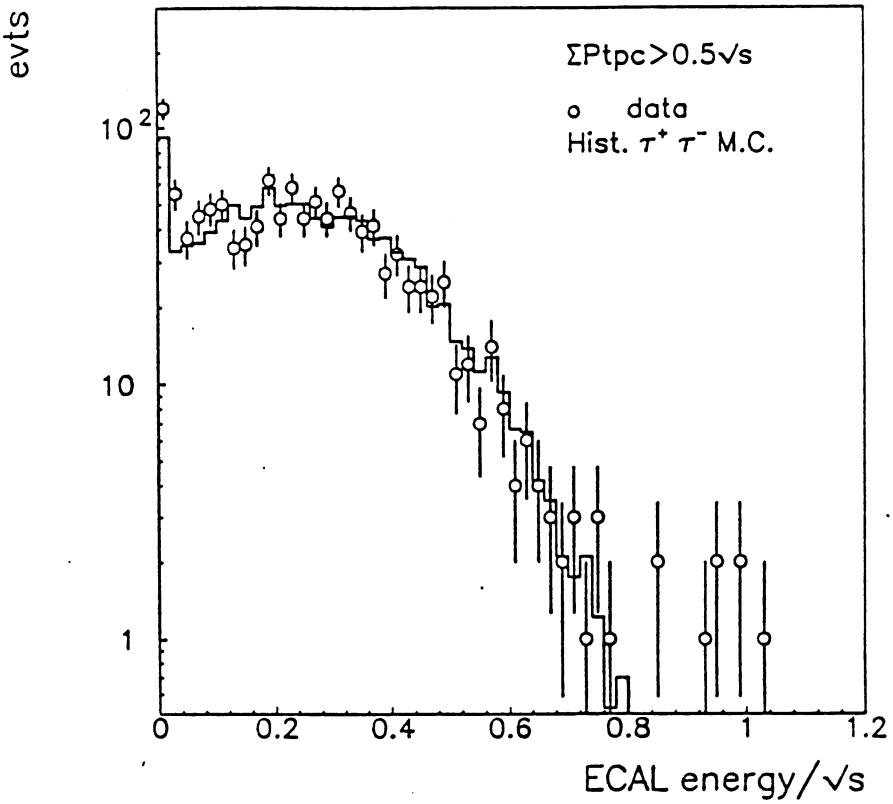
evts
ΣPtpc>0.5√s
o data
Hist. τ⁺ τ⁻ M.C.
10²
10
1
0
0.2
0.4
0.6
0.8
1
1.2
ECAL energy/√s

Figure 28

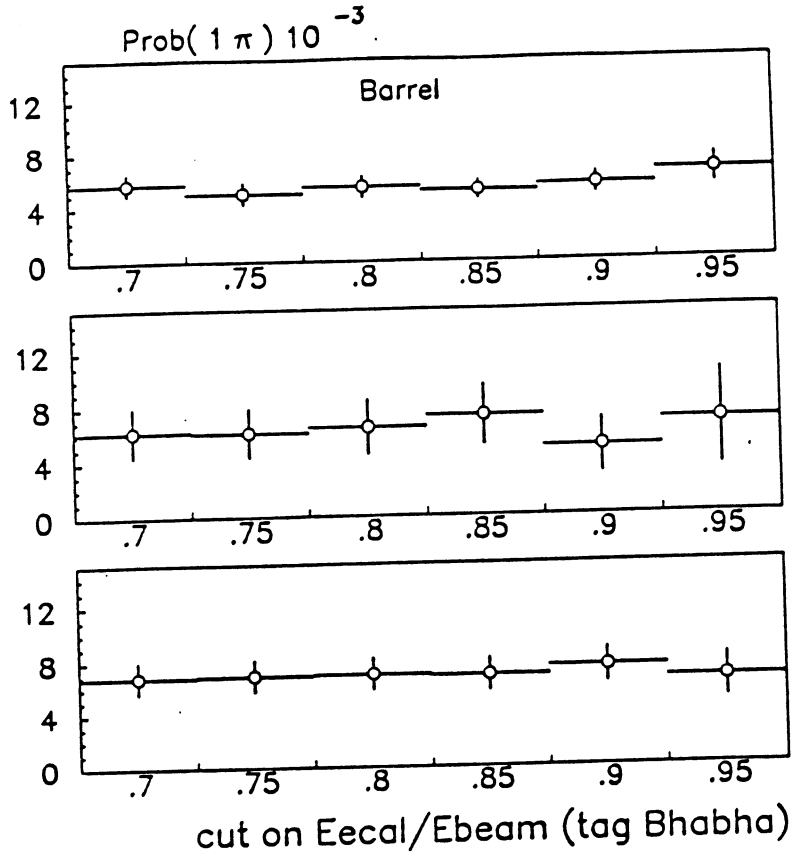
Prob(1 π) 10 -3
Barrel
12
8
4
0
.7
.75
.8
.85
.9
.95
cut on Eecal/Ebeam (tag Bhabha)

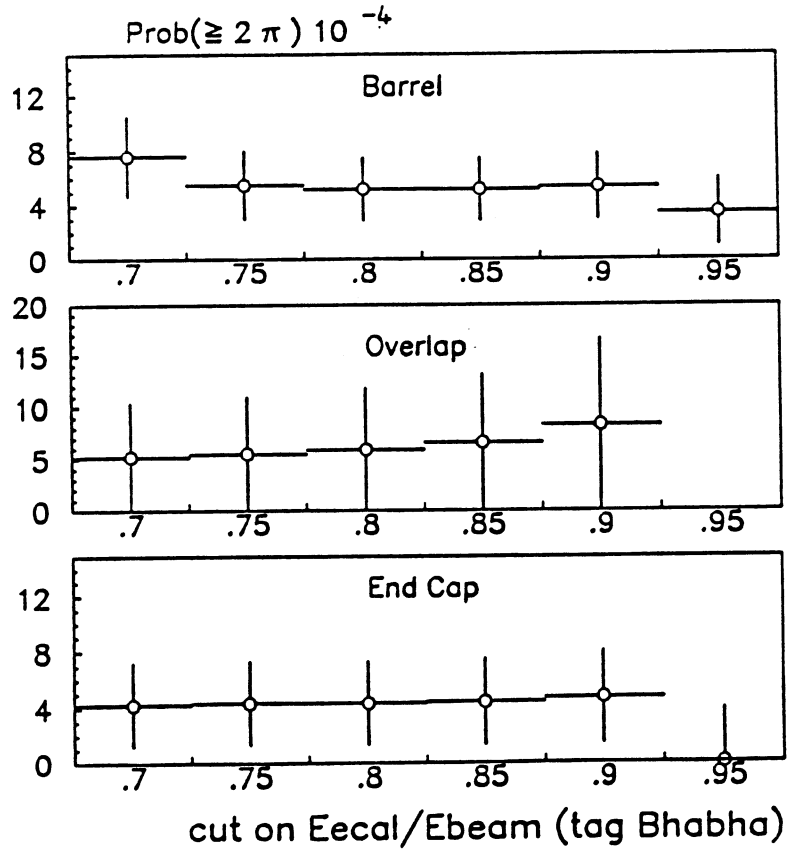
Prob(≧ 2 π) 10 -4
Barrel
Overlap
End Cap
12
8
4
0
20
15
10
5
.7
.75
.8
.85
.9
.95
cut on Eecal/Ebeam (tag Bhabha)

Figure 29

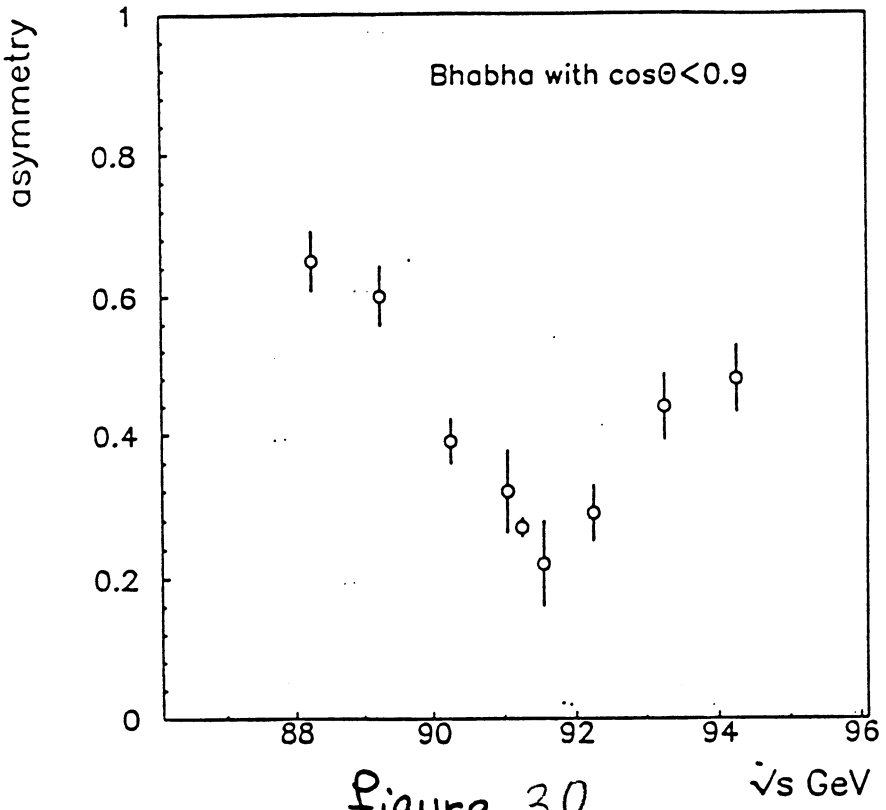
asymmetry
Bhabha with cosΘ<0.9
1
0.8
0.6
0.4
0.2
0
88
90
92
94
96
√s GeV

Figure 30

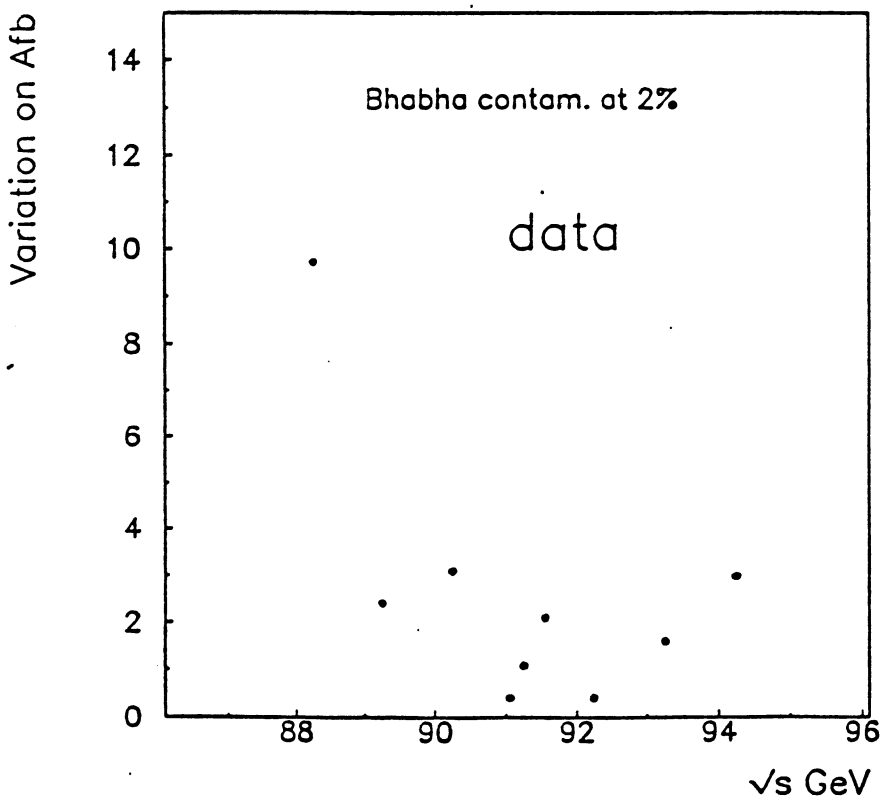
Variation on Afb
Bhabha contam. at 2%
data
14
12
10
8
6
4
2
0
88
90
92
94
96
√s GeV

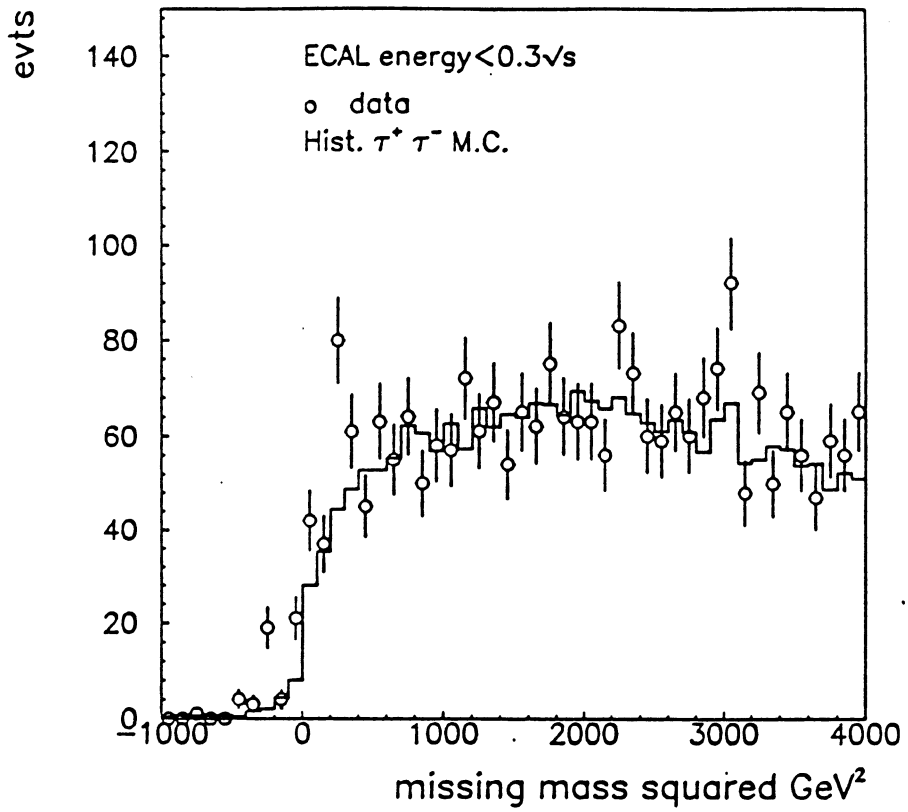
evts
140
120
100
80
60
40
20
0
ECAL energy<0.3√s
o data
Hist. τ⁺ τ⁻ M.C.
-1000
0
1000
2000
3000
4000
missing mass squared GeV²

Figure 31

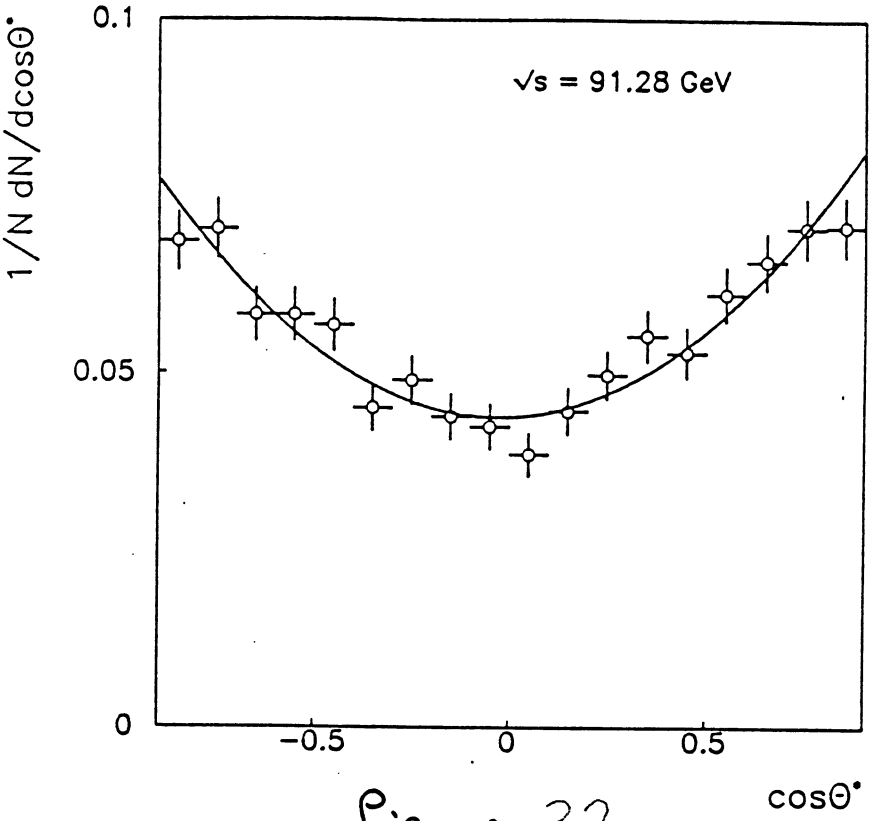

figure 32

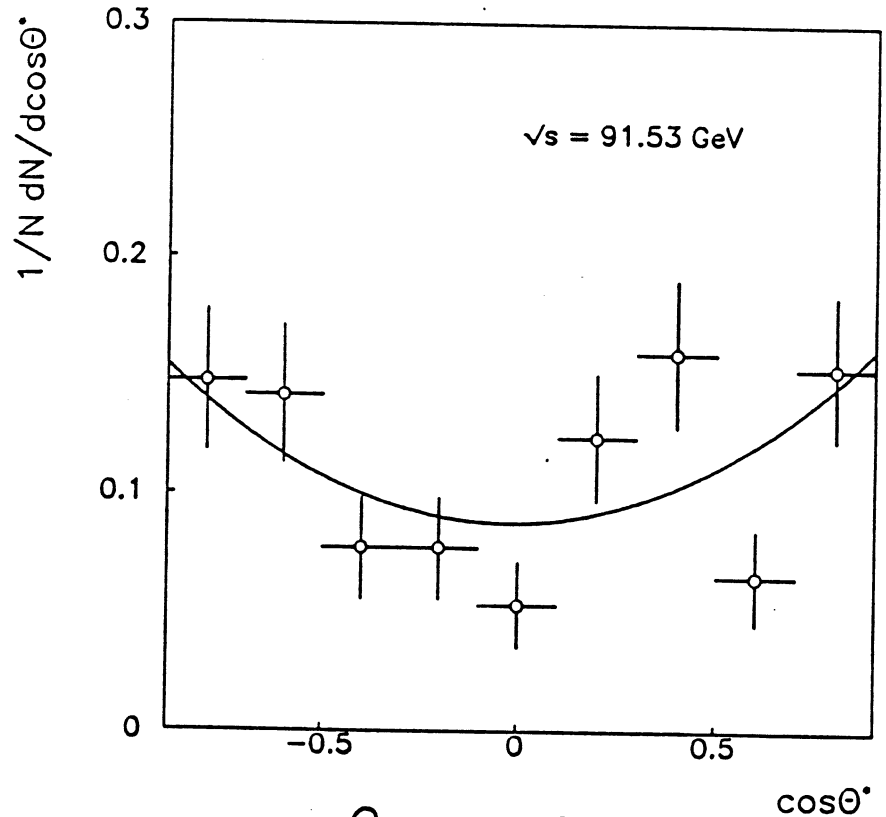

figure 33

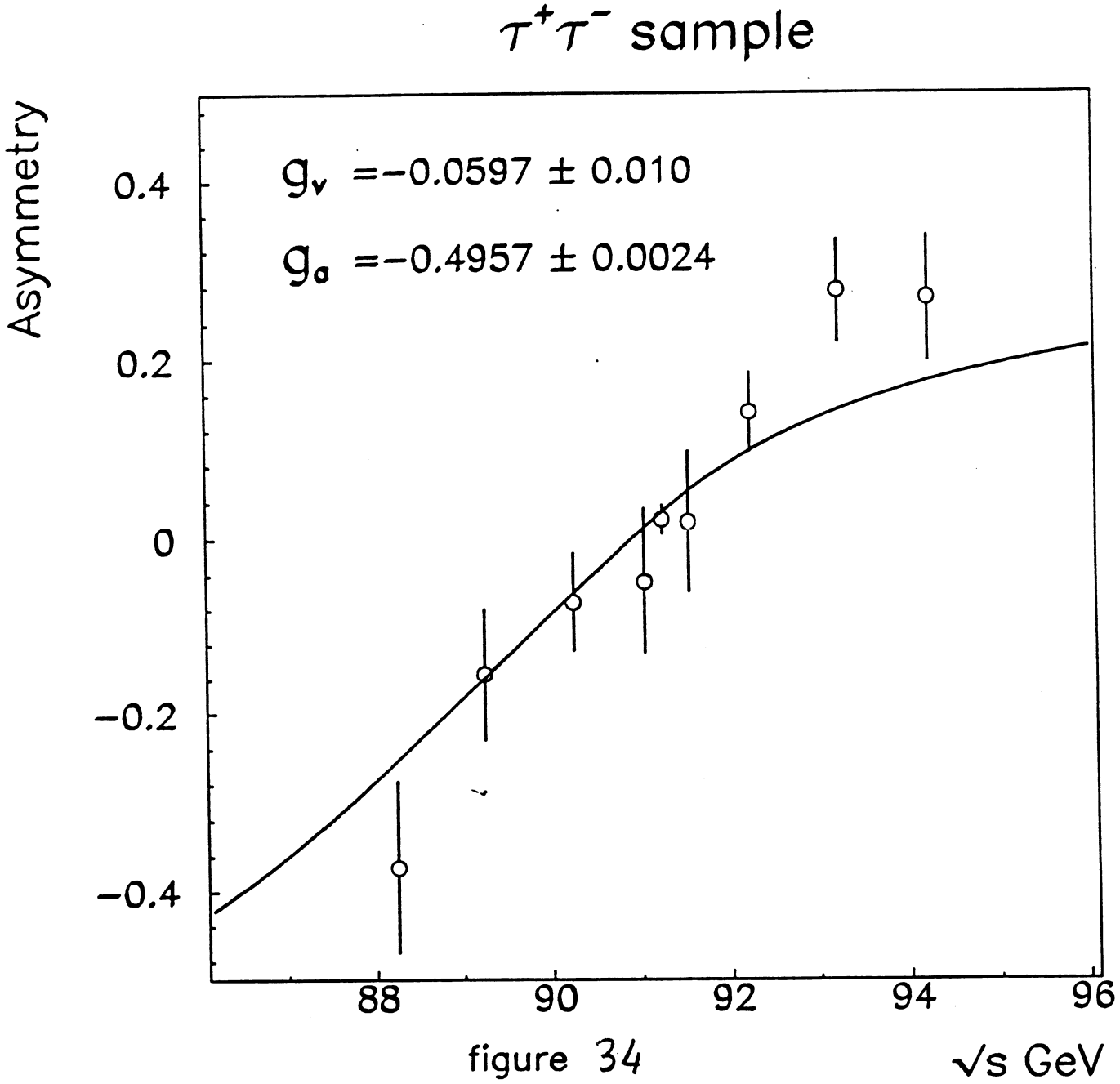
$\tau^+\tau^-$ sample
g_v =−0.0597 ± 0.010
g_a =−0.4957 ± 0.0024
Asymmetry
0.4
0.2
0
−0.2
−0.4
88
90
92
94
96
√s GeV

figure 34